# Channel cross-section heterogeneity of particulate organic carbon transport in the Huanghe

Yutian Ke, Damien Calmels, Julien Bouchez, Marc Massault, Benjamin Chetelat, Aurélie Noret, Hongming Cai, Jiubin Chen, Jérôme Gaillardet, Cécile Quantin

Earth Surf. Dynam., 12, 347–365, 2024
https://doi.org/10.5194/esurf-12-347-2024


Earth Surface Dynamics
Open Access
EGU

# Channel cross-section heterogeneity of particulate organic carbon transport in the Huanghe

**Yutian Ke[1,a], Damien Calmels[1], Julien Bouchez[2], Marc Massault[1], Benjamin Chetelat[3], Aurélie Noret[1], Hongming Cai[2], Jiubin Chen[3], Jérôme Gaillardet[2], and Cécile Quantin[1]**

[1]GEOPS, Université Paris-Saclay-CNRS, 91405 Orsay, France
[2]Institut de Physique du Globe de Paris, Université de Paris, CNRS, 75005 Paris, France
[3]School of Earth System Science, Institute of Surface-Earth System Science, Tianjin University, 300072 Tianjin, China
[a]present address: Division of Geological and Planetary Science, California Institute of Technology, Pasadena, CA 91125, USA

**Correspondence:** Yutian Ke (yutianke@caltech.edu)

Received: 17 May 2023 – Discussion started: 14 June 2023
Revised: 8 December 2023 – Accepted: 21 December 2023 – Published: 15 February 2024

**Abstract.** The Huanghe (Yellow River), one of the largest turbid river systems in the world, has long been recognized as a major contributor of suspended particulate matter (SPM) to the ocean. However, over the last few decades, the SPM export flux of the Huanghe has decreased over 90 % due to the high management, impacting the global export of particulate organic carbon (POC). To better constrain sources and modes of transport of POC beyond the previously investigated transportation of POC near the channel surface, SPM samples were for the first time collected over a whole channel cross-section in the lower Huanghe. Riverine SPM samples were analyzed for particle size and major element contents, as well as for POC content and dual carbon isotopes ($^{13}C$ and $^{14}C$). Clear vertical and lateral heterogeneities of the physical and chemical properties of SPM are observed within the river cross-section. For instance, finer SPM carry more POC in general with higher $^{14}C$ activity near the surface of the right bank. Notably, we discuss how bank erosion in the alluvial plain is likely to generate lateral heterogeneity in POC composition. The Huanghe POC is millennial-aged ($4020 \pm 500$ radiocarbon years) and dominated by organic carbon (OC) from the biosphere, while the lithospheric fraction is ca. 12 %. The mobilization of aged and refractory OC, including radiocarbon-dead biospheric OC, from deeper soil horizons of the loess–paleosol sequence through erosion in the Chinese Loess Plateau is an important mechanism contributing to fluvial POC in the Huanghe drainage basin. Altogether, anthropogenic activities can drastically change the compositions and transport dynamics of fluvial POC, consequentially altering the feedback of the source-to-sink trajectory of a river system to regional and global carbon cycles.

## 1 Introduction

Rivers are the main conveyor of rock and soil debris eroded from the continents to the ocean. Along with inorganic material, river sediments host particulate organic carbon (POC) derived mainly from three major sources: (1) recently photosynthesized OC of the biosphere, (2) aged and altered OC from soils, and (3) ancient OC contained in sedimentary rocks (Blair et al., 2010). The net effect of riverine POC transport on the carbon cycle and thus on the evolution of Earth's climate depends on POC provenance and fate. The effective sedimentary burial of POC derived from the terrestrial biosphere (biospheric OC, $OC_{bio}$) represents a net, long-term sink of atmospheric $CO_2$ (Galy et al., 2007, Bouchez et al., 2014; Hilton et al., 2015), whereas the oxidation of POC derived from continental rocks (petrogenic OC, $OC_{petro}$) acts as a net long-term source of $CO_2$ to the atmosphere (Hilton et al., 2014). The erosion and burial of $OC_{petro}$ escaping from

oxidation has no net effect on the long-term carbon cycle (Galy et al., 2008a; Bouchez et al., 2010; Hilton et al., 2011; Horan et al., 2019). In addition, the reactive nature of $OC_{bio}$ might also result in short-term $CO_2$ emission during transport from both river channels and recently deposited sediments (Mayorga et al., 2005; Galy and Eglinton, 2011; Blair and Aller, 2012).

Globally, rivers transport a total POC flux of ca. $200\,Tg\,C\,yr^{-1}$, consisting of $157^{+74}_{-50}\,Tg\,C\,yr^{-1}$ of $OC_{bio}$ and $43^{+61}_{-25}\,Tg\,C\,yr^{-1}$ of $OC_{petro}$ (Galy et al., 2015; Ludwig et al., 1996). Source-to-sink processes controlling the origin and fate of riverine POC are prominently river-specific, suggesting that the impact of POC on regional and global carbon cycles might significantly vary both spatially and temporally (Blair and Aller, 2012). It is thus crucial to understand the mechanisms controlling the POC export by large rivers that integrate vast portions of the land surface and quantify the differing sources of carbon exported by those large river systems.

The Huanghe (Yellow River) is a highly turbid river system that exports over 85 % of its OC as particulate matter, with efficient deposition and preservation in the ocean (Cauwet and Mackenzie, 1993; Bianchi, 2011; Zhang et al., 2013; Ran et al., 2013). The Huanghe has been highly managed over the last few decades through water and soil conservation measures as well as reservoir construction, leading to a decrease of nearly 90 % of its sediment load (S. Wang et al., 2016, 2007; Milliman et al., 1987) and a significant decrease in its POC delivery to the ocean (Zhang et al., 2013). Reservoir construction dramatically affects the transport and fate of both sediment load and POC in large rivers (Syvitski et al., 2005; Li et al., 2015). The estimated POC flux of the Huanghe is thought to have shifted from $4.5\,Tg\,C\,yr^{-1}$ in the 1980s (Cauwet and Mackenzie, 1993) to 0.34–$0.58\,Tg\,C\,yr^{-1}$ at present (Tao et al., 2018) in response to both anthropogenic influence (Hu et al., 2015; Tao et al., 2018; Yu et al., 2019a) and the natural variability of the regional hydrological cycle (Qu et al., 2020). These large-scale perturbations have likely modified the OC input from the different terrestrial pools and the fate of exported POC that was previously reaching deposition centers in the ocean and that now remains stuck on land. Those alterations of the carbon cycle remain to be addressed.

Over the last decade, POC transport in the Huanghe has been investigated for (1) determination and quantification of POC sources, based on bulk or molecular carbon isotopic composition (Tao et al., 2015; Yu et al., 2019b; Ge et al., 2020; Qu et al., 2020); (2) temporal and spatial variations in POC export and distribution among different size fractions (Ran et al., 2013; X. Wang et al., 2012, 2016; Yu et al., 2019a, b; Qu et al., 2020); (3) impact of anthropogenic activities (Hu et al., 2015; Tao et al., 2018; Yu et al., 2019a); and (4) burial efficiency and preservation in the ocean (Sun et al., 2018; Tao et al., 2016; Ge et al., 2020). However, all these previous studies rely on suspended sediment samples collected near the channel surface or at a single, intermediate depth in the river channel, further assuming a homogeneous distribution of suspended sediment characteristics in the water column, both vertically and laterally. It is now well recognized that suspended sediments present physical, mineralogical, chemical, and isotopic heterogeneities across river transect due to hydrodynamic sorting and tributary mixing (Galy et al., 2008b; Garzanti et al., 2010; Bouchez et al., 2010, 2011a). This is also true for POC, whose age and composition vary following vertical water depth (e.g., Galy et al., 2008b; Bouchez et al., 2014; Hilton et al., 2015; Repasch et al., 2021; Schwab et al., 2022) and lateral river transect (e.g., Bouchez et al., 2014; Baronas et al., 2020) and between sediment size fractions separated in the laboratory (Yu et al., 2019b; Ge et al., 2020). Such heterogeneity warrants a re-evaluation of POC transport in the Huanghe, accounting for the variability in suspended sediment characteristics over the channel cross-section.

In this study, we take advantage of in-river hydrodynamic sorting to access the full range of suspended sediment size fractions by collecting suspended particulate matter (SPM) samples along several river depth profiles distributed across a channel transect (e.g., Bouchez et al., 2014; Freymond et al., 2018; Baronas et al., 2020). We apply this sampling scheme to a cross-section of the Huanghe located 200 km upstream from the river mouth and report SPM OC content, stable isotope composition, and radiocarbon activity, as well as total nitrogen, major element composition (aluminum and silicon), and particle size distribution. Based on these novel samples and data sets, this study aims to (1) determine the controls on POC content in the Huanghe, (2) trace and quantify the sources of riverine POC in the Huanghe, and (3) provide depth-integrated estimates of POC fluxes in the most turbid large river system.

## 2 Study area

The Huanghe originates from the northeastern Qinghai–Tibet Plateau (QTP) and runs through the Chinese Loess Plateau (CLP) and the North China Plain (NCP) to the Bohai Sea (Fig. 1a). It is 5464 km long and drains a basin area of $79.5 \times 10^4\,km^2$. The Huanghe drainage basin can be subdivided into three main geomorphic units: (1) the high-relief upper reaches spanning from the source region (elevation of 4500 m) to the city of Toudaoguai (located 3472 km downstream at an elevation of 1000 m); (2) the middle reaches with a channel length of 1206 km, ending at Huayuankou (elevation of 110 m) draining landscapes characterized by relatively gentle slopes; and (3) the lower reaches where the river flows eastwards across a fluvial plain over a length of 786 km. These three sections drain 53.8 %, 43.3 %, and 2.9 % of the whole Huanghe basin area, respectively (Wang et al., 2007; YRCC, 2016). Most second-order tributaries

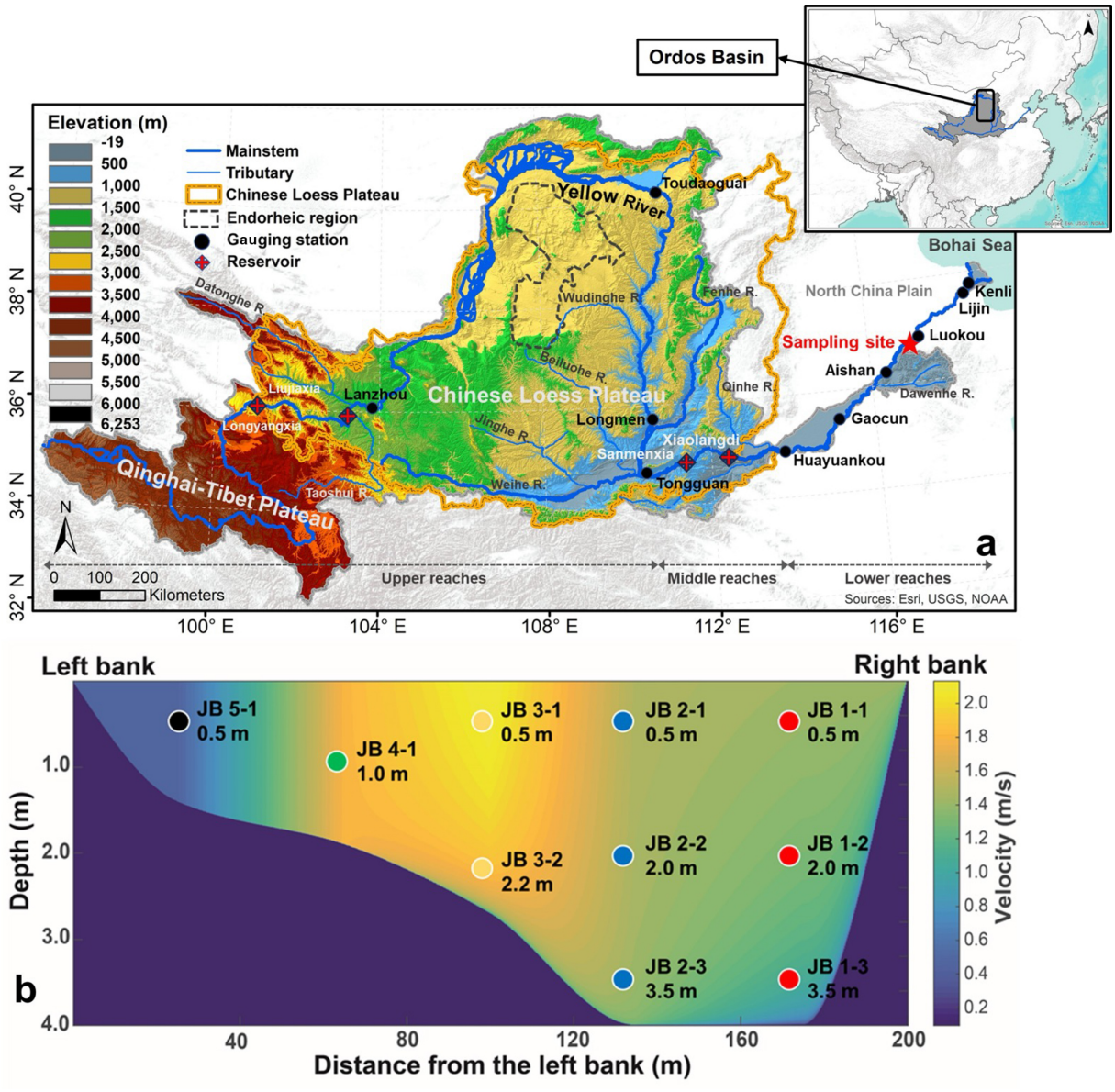


**Figure 1.** **(a)** Elevation map of the Huanghe drainage basin showing the main reservoirs and gauging stations along the main stem and our sampling site (36.75° N, 117.02° E, near the Luokou gauging station). **(b)** Channel cross-section sampled for this study showing the depth and lateral distribution of suspended particulate matter (SPM) samples and modeled velocity distribution based on the "law of the wall" using the point velocity data measured by a current velocity meter attached to the sampler.

drain the CLP region and feed the main channel in the middle reaches, the Dawen River being the only tributary of the lower reaches, with negligible water and sediment supply due to upstream trapping in lakes and reservoirs. It is worth noting that more than 50 % of the water discharge at the Huanghe's mouth comes from the QTP, whereas over 90 % of the sediment load originates from the CLP (Wang et al., 2010, 2017; Pan et al., 2016). The CLP is thus the principal source area of sediment to the Huanghe (Shi and Shao, 2000; Guo et al., 2002; S. Wang et al., 2016).

The Huanghe drainage basin is mostly underlain by the North China craton and is bounded by several mountain belts. The watershed encompasses 46 % of sedimentary rock outcrops (mainly siliciclastic rocks with minor carbonates) and about 45 % of unconsolidated sediments (mainly Quaternary loess deposits). The remaining outcrops include metamorphic, plutonic, and volcanic rocks formed from the Archean to the Tertiary (Fig. S1 in the Supplement). Although river incision is strong in the QTP, a substantial part of the corresponding eroded material is not effectively transferred to the lower reaches due to deposition in the CLP

and the western Mu Us desert, a situation that has prevailed since at least the middle Pleistocene (Nie et al., 2015; Licht et al., 2016; Pan et al., 2016). In addition, recent anthropogenic disturbance such as constructions of large dams in the upper reaches has profoundly modified the export of solid materials from the basin (Wang et al., 2007). The Huanghe then flows through the CLP that has acted as the major supplier of sediment to the system since at least the Calabrian Pleistocene (Stevens et al., 2013; Bird et al., 2015). There, an easily erodible loess–paleosol formation has accumulated since 2.58 Ma (Guo et al., 2002), over a thickness ranging from a few meters to more than 500 m, with an average of 100 m. This loess–paleosol formation and underlying Cretaceous sedimentary rocks are actively incised by the main stem and its tributaries (Shi and Shao, 2000; Guo et al., 2002; S. Wang et al., 2016). Notably, the Ordos Basin underlying the CLP is rich in oil and gas (Guo et al., 2014). In the lower reaches, the river drains Quaternary fluvial deposits and sedimentary rocks.

The Huanghe drainage basin encompasses the entire arid and semi-arid region of northern China in the upper and middle reaches and is characterized by more humid climate conditions in the lower reaches. Annual average precipitation (over the period 1950–2000) in the upper, middle, and lower reaches regions is 368, 530, and 670 mm, respectively (Wang et al., 2007). As a result of the East Asian summer and winter monsoon circulations, the rainy season (June to September) contributes 85 % of the annual precipitation (Wang et al., 2007). During the rainy season, frequent storm events lead to concentrated flows (relatively high discharge) in vulnerable gully–hill systems, the dominant regional geomorphic landscape, and actively participates in soil erosion in the CLP (Shi and Shao, 2000; He et al., 2004; Qu et al., 2020). The present-day (2002 to 2016) suspended sediment flux delivered by the Huanghe to the sea is about $0.12\,\mathrm{Gt\,yr^{-1}}$, which implies a decrease of nearly 90 % in sediment export compared to the widely cited estimate of $1.08\,\mathrm{Gt\,yr^{-1}}$ (average value between 1950 to 1980, Milliman and Farnsworth, 2011). This massive decrease in sediment export mostly results from human perturbations, including soil conservation practices in the CLP and retention in large reservoirs, rather than from climatic variations such as the decreasing precipitation observed in the region over the last decades (Wang et al., 2007; Ran et al., 2013; S. Wang et al., 2016; Li et al., 2022). A scheme for water and sediment regulation (WSR) has been implemented through the construction of the Xiaolangdi Reservoir since 2002, aiming to mitigate water and sediment imbalances in the lower reaches. This regulation has resulted in a modification of the flux of sediment delivered to the lower reaches and estuary, making the Huanghe a highly human-regulated river system. However, no WSR was implemented in 2016, the year of our sampling campaign, suggesting that the collected SPM samples are not significantly affected by retention in dams, and thus they are representative of the fluvial transport of terrestrial materials eroded from the CLP.

## 3 Sampling and analytical methods

### 3.1 Sampling strategy

Detailed sampling of a cross-section of the Huanghe was carried out on the 17 July 2016, during the flood season (Fig. S2 in the Supplement). Samples were collected along five depth profiles near the Luokou hydrological station (36.75° N, 117.02° E), 250 km upstream from the river mouth (Fig. 1). This sampling strategy allows for accessing the full range of suspended sediment particle size (Bouchez et al., 2014). The cross-section is 200 m wide at the surface and 4 m deep at most (Fig. 1; YRCC, 2016). As in previous studies, we used a homemade, 10 L, point sediment horizontal Niskin-type sampler attached to a current velocity meter to collect river water samples and measure the water velocity simultaneously. Subsequently, two water samples were collected at the surface near the right bank in May and June 2017 before the flooding season to retrieve fine suspended particulate matter. For each sample, approximately 30 L of river water was collected and was then filtered through pre-weighed 0.22 µm porosity cellulose acetate membrane filters within 24 h. After rinsing the filters with filtered water, all sediment samples were transferred into centrifuge tubes and freeze-dried before weighing and analysis. A bed sediment (BS) sample was collected on an exposed, recently flooded sediment bar of the riverbed.

### 3.2 Physical and geochemical analysis

Apart from a 50 mg aliquot of SPM samples preserved for particle size analysis, samples were finely ground using an agate mortar and pestle prior to chemical and isotopic analyses. The particle size distribution of the unground aliquots was measured using a laser diffraction particle size analyzer (Beckman Coulter LS-12 320) at the École Normale Supérieure (ENS), Paris, France. Before analysis, unground SPM aliquots were dispersed in deionized water and then in sodium hexametaphosphate in an ultrasonic bath. For each sample, we measured three replicates and report the average median particle size (D50, µm) with an uncertainty better than 2 % (Table 1). The chemical composition of SPM samples was measured on ground aliquots at the Centre de Recherches Pétrographiques et Géochimiques (CRPG), Vandoeuvre-lès-Nancy, France, using inductively coupled plasma atomic emission spectroscopy (ICP-OES) for major elements with typical uncertainties of 3 % (Carignan et al., 2001).

For particulate organic carbon content (POC %, wt.), stable carbon isotope $\delta^{13}C$ (in $‰_{VPDB}$, i.e., in ‰ relative to Vienna Pee Dee Belemnite), and radiocarbon isotope $\Delta^{14}C$ (expressed as fraction modern, $F_m$), ground homogenized sam-

**Table 1.** SPM characteristics and POC properties of the river cross-section sampling.

| Sample ID | Type | Depth (m) | SPM ($mg L^{-1}$) | POC (%) | SD | $\delta^{13}C_{org}$ (‰) | SD | $F_m$ | $\Delta^{14}C$ (‰) | SD | $^{14}C$ age | TN (%) | $N/C_{org}$ | Al/Si | D50 (µm) |
|---|---|---|---|---|---|---|---|---|---|---|---|---|---|---|---|
| JB 1-1 | SPM | 0.5 | 679 | 0.44 | 0.02 | −25.84 | 0.03 | 0.645 | −360 | 7 | 3527 | 0.078 | 0.178 | 0.243 | 19.5 |
| JB 1-2 | SPM | 2 | 757 | 0.45 | 0.01 | −25.80 | 0.06 | 0.613 | −392 | 11 | 3929 | 0.080 | 0.179 | 0.238 | 23.7 |
| JB 1-3 | SPM | 3.5 | 1095 | 0.39 | 0.01 | −26.13 | 0.04 | 0.675 | −331 | 7 | 3161 | 0.077 | 0.197 | 0.216 | 34.5 |
| JB 2-1 | SPM | 0.5 | 730 | 0.40 | 0.03 | −26.00 | 0.01 | 0.631 | −374 | 7 | 3703 | 0.069 | 0.175 | 0.255 | 39.8 |
| JB 2-2 | SPM | 2 | 1124 | 0.32 | 0.01 | −26.37 | 0.06 | 0.569 | −436 | 13 | 4537 | 0.050 | 0.156 | 0.196 | 60.4 |
| JB 2-3 | SPM | 3.5 | 1806 | 0.29 | 0.01 | −26.53 | 0.06 | 0.552 | −453 | 38 | 4779 | 0.042 | 0.144 | 0.172 | 86.0 |
| JB 3-1 | SPM | 0.5 | 1058 | 0.32 | 0.02 | −26.09 | 0.03 | 0.582 | −422 | 12 | 4346 | 0.058 | 0.181 | 0.190 | 50.1 |
| JB 3-2 | SPM | 2.2 | 2459 | 0.31 | 0.02 | −26.55 | 0.04 | 0.589 | −415 | 11 | 4247 | 0.049 | 0.159 | 0.186 | 73.1 |
| JB 4-1 | SPM | 1 | 1747 | 0.41 | 0.02 | −25.75 | 0.06 | 0.630 | −375 | 8 | 3714 | 0.073 | 0.175 | 0.217 | 29.0 |
| JB 5-1 | SPM | 0.5 | 1406 | 0.32 | 0.01 | −26.12 | 0.05 | 0.589 | −416 | 11 | 4256 | 0.061 | 0.188 | 0.186 | 58.2 |
| HH 17.05 | SPM | 0 | 83 | 0.92 | 0.00 | −25.73 | 0.14 | 0.711 | −295 | 19 | 2740 | 0.184 | 0.200 | 0.358 | 5.2 |
| HH 17.06 | SPM | 0 | 54 | 1.21 | 0.01 | −25.60 | 0.07 | 0.729 | −277 | 25 | 2539 | 0.261 | 0.215 | 0.377 | 4.3 |
| HH | BS | | | 0.21 | 0.03 | −27.35 | 0.05 | 0.099 | −901 | 7 | 18539 | 0.019 | 0.087 | 0.175 | 44.4 |

ples were fumigated using 12M HCl fumes in a closed Teflon tank at 60 °C for 48 h to remove the carbonate fraction, and were then dried under vacuum prior to analysis. Total nitrogen content (TN %, wt.) was measured on non-acidified samples (Komada et al., 2008). Triplicate analysis on POC % and $\delta^{13}C$ of POC (acidified aliquots), as well as TN % (non-acidified aliquots), were carried out on an organic elemental analyzer (OEA) coupled with isotope ratio mass spectrometry (IRMS, Thermo Scientific Flash 2000) under continuous-flow mode at Géosciences Paris Saclay (GEOPS), Orsay, France. Subjected to the blank subtraction by linearity test, two international standards including USGS-40 and IAEA-600 in addition to an internal standard (GG-IPG) were used to build linear regression equations to calibrate the elemental and isotopic values for both carbon and nitrogen. Uncertainties in POC %, $\delta^{13}C$, and TN % based on replicate measurements ($1\sigma$, $n = 3$) are lower than 0.02 %, 0.06 ‰, and 0.02 ‰, respectively. The $^{14}C$ activity of POC was measured on a new compact accelerator mass spectrometry (AMS) device, ECHoMICADAS (Hatté et al., 2023), using a gas ion source interface system (GIS) at the Laboratoire des Sciences du Climat et de l'Environnement (LSCE), Gif-sur-Yvette, France, with an absolute uncertainty of max ± 0.5 %. Aside from the gas bottles of prepared blank PhA and standard NIST OX II that are permanently connected to the GIS and used for normalization and corrections for fractionation and background, international standards including IAEA-C5, IAEA-C7, IAEA-C8, and blank PhA were prepared in different sizes (10 to 100's µg C) to match the amount of OC found in the sediment samples.

### 3.3 POC source apportionment

To quantify the contribution and associated uncertainties of various sources to POC transported in the Huanghe, a Bayesian Markov Chain Monte Carlo (MCMC) approach based on a mixing scheme with three end-members (Appendix A) was adopted. This approach considers the variability of each end-member contribution, assuming this variability can be represented by a normal distribution. We computed the a posteriori distribution of the Bayesian formulation using the MCMC method using the MixSIAR package (Moore and Semmens, 2008; Stock and Semmens, 2016). All computations were performed in the R environment (http://www.r-project.org/, last access: 3 December 2023). To ensure reliable simulation, the model was run with a chain length of 300 000 by 3 chains, using a burn-in of 200 000 steps and a data thinning of 100 for each sample. The mixing model was constructed on the dual stable and radioactive isotope of the riverine POC pool ($\delta^{13}C$ and $\Delta^{14}C$) and of the three potential source pools (Sect. 5.2) by the following equations:

$$\text{Isotope\_ratio}_{\text{sample}} = \sum_{\text{source}} \left(f_{\text{source}} \cdot \text{Isotope\_ratio}_{\text{source}}\right)$$
$$\sum_{\text{source}} f_{\text{source}} = 1$$

where $\text{Isotope\_ratio}_{\text{sample}}$ is either the $\delta^{13}C$ or $\Delta^{14}C$ value of the sample, $\text{Isotope\_ratio}_{\text{source}}$ is either the $\delta^{13}C$ or $\Delta^{14}C$ value of different possible sources of POC, and $f_{\text{source}}$ is the relative contribution of each source of POC. Further model diagnostics were performed using Gelman–Rubin and Geweke tests, with both diagnostics having validated the robustness and convergency of the model.

### 3.4 Depth-integrated fluxes

Instantaneous depth-integrated fluxes of SPM and POC sources were calculated for the cross-section using a method developed by Bouchez et al. (2011a, b). This method is based on the systematic variation of SPM concentration in the water column (Fig. 2) applying a Rouse-based model (Rouse, 1937). We first constructed a bathymetric profile of the river cross-section based on the depth information collected in

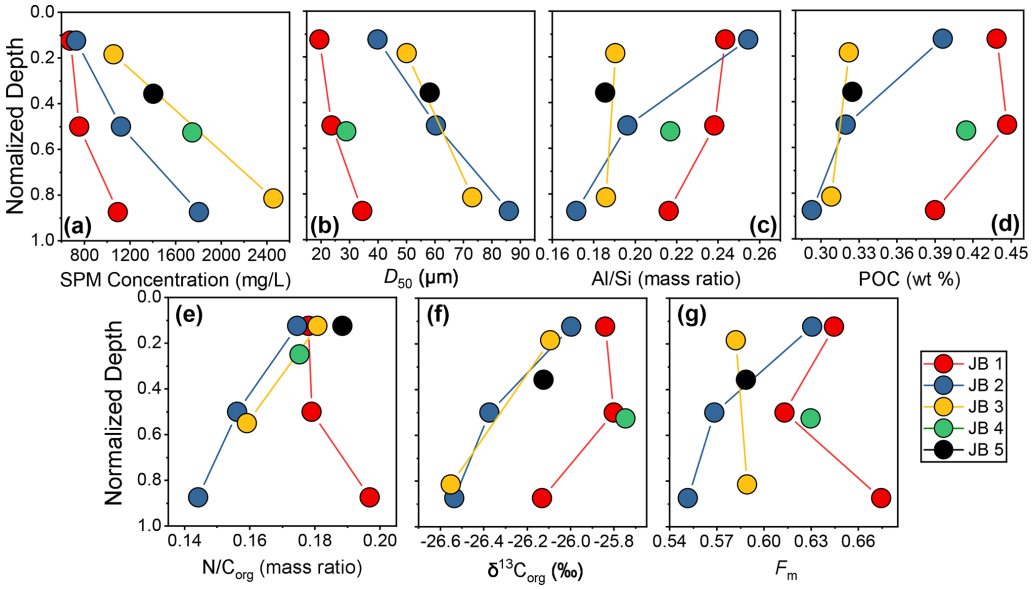


**Figure 2.** Variation in physical and chemical parameters in the river cross-section, shown as a function of sampling depth normalized to total depth of the water column at the location of the considered depth profile, for the Luokou cross-section on the Huanghe (16 June 2017): **(a)** SPM concentration, **(b)** particle size distribution (shown as D50), **(c)** Al/Si mass ratio, **(d)** POC content (weight %), **(e)** N/$C_{org}$ mass ratio, **(f)** stable carbon isotope ratio $\delta^{13}C_{org}$ (‰), and **(g)** radiocarbon activity $F_m$.

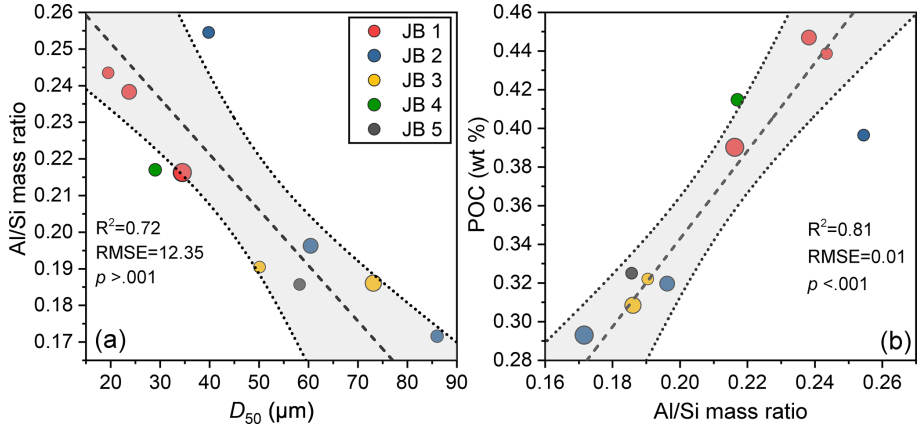


**Figure 3.** Relationships between **(a)** particle size D50 and Al/Si mass ratio. **(b)** Al/Si mass ratio and POC content for the Luokou cross-section on the Huanghe (17 July 2016). The symbol size indicates the sampling depth in the water column, with symbol size increasing with depth. The shaded area represents the 95 % confidence area of the linear best fit (dashed black line); the upper and lower bounds are marked by dotted grey lines.

the field and then modeled the velocity distribution across the transect (Fig. 1b) through fits of the so-called "law of the wall" to water velocity measured at the location of each sample within the cross-section using a current meter (Garcia, 2008). Afterward, the concentration of total SPM and various particle size fractions could be estimated by applying the so-called Rouse model (Rouse, 1937) to each particle size fraction separately (Bouchez et al., 2011a), resulting in a map of the particle size distribution in the river cross-section (Fig. S3 in the Supplement). The aluminum-to-silicon ratio (Al/Si mass ratio) is inversely related to the particle size of river SPM in the Ganges–Brahmaputra, Amazon, and Mackenzie rivers (Galy et al., 2007; Bouchez et al., 2014; Hilton et al., 2015). Such a linear relationship between D50 and Al/Si was also observed in our dataset, allowing for computing the spatial distribution of POC content in the cross-section, based on the linear relationship between POC and Al/Si (Fig. 3). Finally, combining modeled water velocity, SPM concentration, and POC distribution we calculated a depth-integrated, instantaneous POC flux for the whole river channel (Fig. S3, detail in the Supplement).

## 4 Results

We report the first isotopic dataset of POC samples collected along several depth profiles distributed over a cross-section of the Huanghe (Table 1, $n = 10$). SPM concentrations range from 679 to 2459 mg $L^{-1}$ (avg. $1286 \pm 572$ mg $L^{-1}$, reported with a mean value with 1 standard deviation hereafter) and show an obvious increase from the surface to the bottom and from the right bank to the left bank (Figs. 1b and 2a). The surface SPM concentration (i.e., samples collected 0.5 m below the surface) decreases laterally as the water column deepens. The range of measured Huanghe SPM D50, i.e., the median particle size (19.5–86.0 µm, Fig. 2b), agrees with that of SPM collected at Lijin (16.6–120.1 µm, $n = 50$) during the same flooding season by Moodie et al. (2022). In each depth profile, SPM is consistently coarsening with depth as revealed by the evolution of grain size parameters such as D10, D50, and D90 (Tables 1 and S1 in the Supplement, Figs. 2 and S4 in the Supplement). The finest SPM is transported on the right bank and at the surface, while the coarsest SPM is found at the bottom of the middle profile (sample JB 2-3). Two types of depth profiles can be distinguished at Luokou based on particle size distributions (Fig. S4) and the relationship between D50 and water depth (Fig. 2b). On the one hand, the JB 1 and JB 4 profiles show a well-marked, bi-modal distribution of particle size (Fig. S4) together with relatively low and consistent D50 (Fig. 2b). On the other hand, the JB 2, JB 3, and JB 5 profiles show a more unimodal distribution of particle size (Fig. S4) and a unique D50–sampling depth relationship (Fig. 2b). Interestingly, these two groups can also be distinguished in terms of relationships between POC % and $\delta^{13}C$ with water depth (Fig. 2d and f). As expected, the Al/Si ratio is closely related to the particle size, and the ratios measured in the middle profile SPM samples (0.17 for JB 2-3 and 0.26 for JB 2-1) encompass the full range of Al/Si found in the whole cross-section (Fig. 2c). The relatively low Al/Si ratios are comparable to that of the middle Huanghe (Qu et al., 2020) and other large turbid river systems such as the Ganges–Brahmaputra (Galy et al., 2008b), Salween, and Irrawaddy (Tipper et al., 2021).

SPM in the Huanghe is characterized by low TN and POC content (wt.%), ranging from 0.04 % to 0.08 % ($0.06 \pm 0.01$ %) and from 0.29 % to 0.42 % ($0.37 \pm 0.06$ %), respectively (Fig. 2d; Table 1). POC content generally decreases from the surface to the riverbed, with quantitative differences from one profile to another (Fig. 2d). Notably, the JB 1 profile shows the highest POC % and TN %. In addition, the ratio of TN % to POC %: $N/C_{org}$ increases with depth in the JB 1 profile (from top to bottom), while it decreases in the JB 2 and JB 3 profiles (Fig. 2e). The $\delta^{13}C$ of POC varies over a narrow range from −26.55 ‰ to −25.75 ‰ ($-26.12 \pm 0.29$ ‰, Fig. 2f) and becomes lighter with depth, showing that fine SPM has higher $\delta^{13}C$ than coarse SPM. These values are lower than those previously reported for other Huanghe sampling sites upstream: $-24.7 \pm 0.4$ ‰ at Toudaoguai, $-24.9 \pm 0.6$ ‰ at Longmen, and $-23.8 \pm 0.6$ ‰ at Lijin (Qu et al., 2020, Hu et al., 2015; Tao et al., 2015; Yu et al., 2019a; Ge et al., 2020). The radiocarbon activity of POC of the Huanghe at Luokou is relatively low (Fig. 2g), with $F_m$ ranging from 0.552 ($\Delta^{14}C = -453$ ‰; sample JB2-3) to 0.675 ($\Delta^{14}C = -331$ ‰; sample JB1-3), spanning from 3160 to 4780 $^{14}C$ years, and the average value is $0.607 \pm 0.038$ ($\Delta^{14}C = -412 \pm 37.6$ ‰, $n = 10$). This range of radiocarbon activity is consistent with published values for POC collected at the river surface downstream of Toudaoguai (Qu et al., 2020). All the POC radiocarbon activity data reported so far for the Huanghe are comparable to mean values for Arctic large rivers ($\Delta^{14}C = -397$ ‰, ca. 4480 $^{14}C$ years, Ke et al., 2022), revealing the multimillennial-aged nature of POC transported by the Huanghe. The elemental and isotopic signatures of the two fine SPM samples HH 17.05 and HH 17.06 (on average POC % = 1.07 %, $\delta^{13}C = -25.67$ ‰, $F_m = 0.720$, and Al/Si = 0.37) are significantly different from those of the depth profile samples (Table 1). The bed sediment sample has a comparatively low POC % (0.21 %), $\delta^{13}C$ (−27.35 ‰), $F_m$ (0.099), and Al/Si ratio (0.17).

## 5 Discussion

We observe significant heterogeneities of elemental and isotopic carbon composition as well as inorganic chemistry over the studied river cross-section. The possible mechanisms behind these variations are assessed hereafter. Then, sources of riverine POC are determined and quantified, confirming that erosion of the loess–paleosol sequence of the CLP is a major source of aged and refractory biospheric OC to the Huanghe. Finally, we assess the POC load and its variability over the transect profile, inferring the importance of the supply of POC from the river bottom in the Huanghe.

### 5.1 Transportation mode of POC in the Huanghe

#### 5.1.1 POC loading and its controls

The Huanghe is characterized by a high SPM load with relatively low POC % ($0.37 \pm 0.06$ %, $n = 10$). In the Luokou cross-section, POC content generally increases with decreasing particle size (Fig. S5 in the Supplement), with the two clay-sized ("HH") samples showing the largest POC content (Table 1). Consistently, the Al/Si ratio of Huanghe sediments, which varies as an inverse linear function of the median particle sizes D50 ($R^2 = 0.72$, $p > 0.001$, Fig. 3a), positively correlates with POC % ($R^2 = 0.81$, $p < 0.001$ Fig. 3b), a pattern observed globally (Galy et al., 2008b; Bouchez et al., 2014; Hilton et al., 2015; Repasch et al., 2021). This pattern is consistent with POC variability in the Huanghe reported for manually separated size fractions of sediments (Yu et al., 2019b).

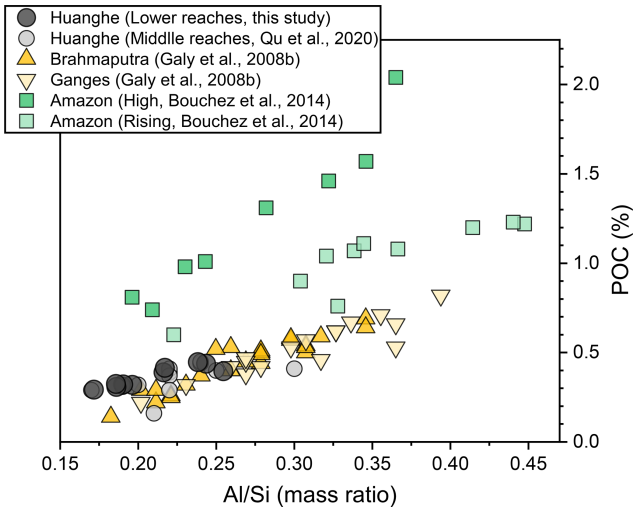


**Figure 4.** "POC loading" of river SPM of large rivers. The POC loading is estimated from the slope of the relationship between POC content and the Al/Si ratio of each fluvial system (Galy et al., 2008b). All SPM samples were collected along depth profiles except for the middle Huanghe (Qu et al., 2020).

The first reason for the low POC content of Huanghe sediments is therefore their relatively low values of Al/Si compared to other systems – a feature that can be related to the quartz-rich, OC-poor nature of the loess–paleosol formations of the CLP (Jahn et al., 2001; Huang and Ren, 2006; He et al., 2006; Ning et al., 2006; S. Wang et al., 2016). However, Huanghe sediments are relatively poor in POC, even considering their low Al/Si, compared to other rivers globally. To that effect, the so-called "POC loading" can be characterized by the slope described by sediment data in an Al/Si POC diagram (Galy et al., 2008b; Fig. 4). For a given Al/Si ratio, the POC % in the Luokou cross-section is similar to that of the middle Huanghe (Qu et al., 2020), indicating the relatively invariant transport mode of POC between the middle and lower reaches. Previous studies have shown that the positive relationship between POC % and Al/Si can be partially explained by OC adsorption onto the mineral surface (Curry et al., 2007; Galy et al., 2008b; Blair and Aller, 2012; Bouchez et al., 2014; Qu et al., 2020). In the loess–paleosol deposits acting as a source of sediments to the Huanghe, OC is mostly preserved and stabilized by forming organo-aggregates with kaolinite and through adsorption onto iron oxides (Wang et al., 2013).

However, POC loading in the Huanghe is small compared to that of the Amazon (Bouchez et al., 2014), but similar to that of the Ganges-Brahmaputra system (Galy et al., 2008b). While many factors could influence POC loading across these catchments, we note that another similarity between the Huanghe and Ganges–Brahmaputra fluvial systems is their millennial-aged $OC_{bio}$ (Galy et al., 2007; Tao et al., 2016). This is in stark contrast with the Amazon, where younger $OC_{bio}$ ages have been reported (Bouchez et al., 2014). Given that younger $OC_{bio}$ recently photosynthesized in terrestrial or aquatic ecosystems can be readily oxidized within catchments (Mayorga et al., 2005), the relatively low POC loading observed at the mouth of the Ganges–Brahmaputra and the Huanghe (Fig. 4) could be related to the predominance of refractory, aged $OC_{bio}$ and $OC_{petro}$ in those systems, while the Amazon sediments would still contain significant amount of younger, more labile $OC_{bio}$.

In detail, and as explained in more detail below (Sect. 5.1.2), we also observe a significantly different POC loading between the JB 1 and JB 2 depth profiles at the Luokou station (Fig. 3). This difference in POC loading in the cross-section of the Huanghe might indicate the delivery of recent $OC_{bio}$, specifically near the right bank (the closest to the JB 1 profile) for the Luokou site, a scenario that is supported by the comparatively younger age of POC in profile JB 1. Consistent with this interpretation, temporally variable POC loading at a given site has been reported for the Amazon (Bouchez et al., 2014), where higher POC loading during the high-water stage compared to the rising water stage has been attributed to the erosion of discrete organic debris from riverbanks.

Variable POC loading amongst large catchments has implications for evaluating the likelihood of POC preservation in estuaries. The Ganges-Brahmaputra system delivers relatively old, refractory $OC_{bio}$ to the Bengal Fan with an almost complete burial efficiency (Galy et al., 2007). Given the observed similarity in POC loading and age, we can thus expect a similar, efficient preservation for the Huanghe offshore depositional system. In addition to the low reactivity of the POC transported by the Huanghe, the high sediment accumulation rates in the Huanghe coastal domain might further inhibit OC oxidation (Blair and Aller, 2012). Consequently, the case of the Huanghe differs drastically from that of the Amazon, where higher POC loading is observed, with a larger contribution of young, labile $OC_{bio}$ either as discrete organic matter or associated with mineral surfaces, leading to low POC burial efficiency in the ocean (Bouchez et al., 2014; Blair and Aller, 2012).

### 5.1.2 Chemical heterogeneity within the transect

There is clear lateral and vertical variability of POC content and SPM inorganic chemistry across the Luokou cross-section of the Huanghe. For each vertical depth profile, clay-rich fine particles are transported near the channel surface and quartz-rich coarse particles flow near the river bottom. Accordingly, the Al/Si ratio, POC content, and POC radiocarbon activity generally decrease with depth. Elemental (POC %) and isotopic POC signatures ($^{13}C$ and $^{14}C$) are inversely related to the particle size (D50; Fig. S5). These patterns are observed in other large fluvial systems, e.g., Ganges and Brahmaputra, Amazon, and Mackenzie (Galy et al., 2008b; Bouchez et al., 2014, Hilton et al., 2015),

showing that hydrodynamic sorting is the primary control on suspended sediment OC content, segregating inorganic and organic material according to particle size (Bouchez et al., 2011a, 2014).

At the Luokou sampling site, lateral variability at the channel surface shows that POC-rich fine particles are preferentially transported near the right bank (Figs. 2 and S3). This pattern is validated by the Rouse model provided in Sect. S1 in the Supplement, the Rouse number ($Z_R$) is 0.137, 0.236, and 0.284 for JB-1, JB-2, and JB-3, respectively. In essence, $Z_R$ can reflect the balance between gravitation settling and upward turbulent diffusion. $Z_R$ is smaller near the right bank and larger near the left bank, showing heterogeneity across the transect. Larger particles exhibit a faster settling velocity due to their increased weight, leading to a higher $Z_R$. On the other hand, the lighter ones settle more slowly, resulting in $Z_R$ approaching 0. This means that their concentration remains relatively constant along a given depth profile. However, as depth increases and the concentration of larger particles grows, the proportion of these finer particles in the overall sediment decreases (Bouchez et al., 2011a). The channel geometry thus needs to be examined as a potential factor to produce such lateral heterogeneity, in particular the mechanisms of bed sediment resuspension and bank erosion.

Resuspension of bed sediments is also a possible mechanism that could explain the lateral heterogeneity in POC content in the study cross-section of the Huanghe. Indeed, scouring of channel bed sediment at high water flow may also shift POC to more negative radiocarbon and stable isotope signatures. Our sample set collected in July 2016 during a flooding period (water flow velocity up to 2.1 $m\,s^{-1}$, Fig. 1) supports this scenario. Indeed, the increase in D50 of surface SPM samples from right to the left bank, i.e., with total channel depth decrease, is consistent with coarse-sediment resuspension from the bed. This is also supported by the Rouse model, where higher $Z_R$ in the shallow water near the left bank indicates a greater likelihood of sediment settling to the bed, lower $Z_R$suggests that there is enhanced SPM supply from the riverbed. Such a scenario is also supported by the 3-fold increase in SPM flux observed from the upstream Huayuankou station to the downstream Lijin station in July 2016, despite a 4-fold decrease in water discharge (Fig. S2).

Bank erosion can be a significant mechanism for the delivery of sediments to river systems (Guo et al., 2007). Bank erosion at Luokou would make OC from the lower Huanghe alluvial plain a potential source of POC in the lower reaches of the Huanghe. Frequent inundation to the adjacent riparian zones in flooding seasons, surface runoff driven by storm events, and agriculture irrigation, etc., can mobilize young soil OC and discrete organic matter debris (e.g., plant-derived debris) to riverine POC (Hilton et al., 2011; Turowski et al., 2016). This mechanism provides a possible explanation for the opposite trends displayed by samples from the JB 1 and JB 2 profiles in the $F_m$ vs. $\delta^{13}C$ space (Fig. 5). The youngest POC was found at the bottom of the JB 1 profile (JB 1–3). Meanwhile, the JB 1 samples have comparatively higher $N/C_{org}$ ratios and N%, consistent with the input of discrete plant-derived debris from the bank in addition to rock-derived detrital clastic material in the coarse fractions (> 32 µm, Yu et al., 2019b). The transport and entrainment of plant debris deep in the water column has been evidenced in many large river systems, such as the Amazon (Feng et al., 2016), the Ganges–Brahmaputra (Lee et al., 2016), the Mackenzie (Schwab et al., 2022), and the Rio Bermejo rivers (Repasch et al., 2021). Such input would also provide an explanation for the higher POC loading of the JB 1 profile (Sect. 5.1.1).

## 5.2 POC provenance in the Huanghe: the significance of loess–paleosol-derived OC

### 5.2.1 Physical erosion of the loess–paleosol sequence

Over decennial to centennial timescales, the POC export of the Huanghe is mainly controlled by erosion of the CLP. Throughout the Quaternary, the erosion rate in the Huanghe basin has been mainly driven by climate shifts until human activities started and profoundly impacted sediment fluxes in the mid-Holocene (He et al., 2006). The Huanghe has experienced a 90 % decrease in annual sediment load since the 1950s (S. Wang et al., 2016), caused by weakened soil erosion to the CLP and sediment retention by dams (Wang et al., 2007; Ran et al., 2013; S. Wang et al., 2016; Li et al., 2022). To determine the contributions of the various terrestrial OC components to Huanghe POC, we compiled published POC carbon isotope data for sediments collected in the lower reaches from 2011 to 2016, after the Xiaolangdi Reservoir began operation (Figs. 5 and 6). This dataset shows that the radiocarbon ages of Huanghe POC are considerably old ($5100 \pm 1700$ $^{14}C$ years, $n = 29$), with a minor fraction of modern photosynthesized $OC_{bio}$ (Tao et al., 2015; Yu et al., 2019a, b). This relatively $^{14}C$-depleted POC suggests the significant contribution of OC originated from deep soil horizons within the catchment. Given that loess is easily erodible and that there is widespread gully erosion in the catchment, more intensive erosion of the CLP can mobilize more soils as well as older OC from deep soil horizons to fluvial transport. Therefore, higher sediment load in the river can be characterized by radiocarbon-depleted POC. This is evidenced by the negative trend between $^{13}C$ and $F_m$ of POC for sediment samples collected in the Huanghe over the 2011–2016 period (Fig. 5a), suggesting that deep horizons of the loess–paleosol formations are a plausible source for the $^{14}C$-depleted end-member. Besides, the preferential erosion of bomb-carbon-affected, recently photosynthesized, and possibly degraded $OC_{bio}$ from the overlying topsoils (< 10 cm) most likely contributes to riverine POC (Tao et al., 2015).

As such, variable contribution of aged and radiocarbon-free OC from deep horizons of loess–paleosol formations of the CLP should have a significant impact on the elemental

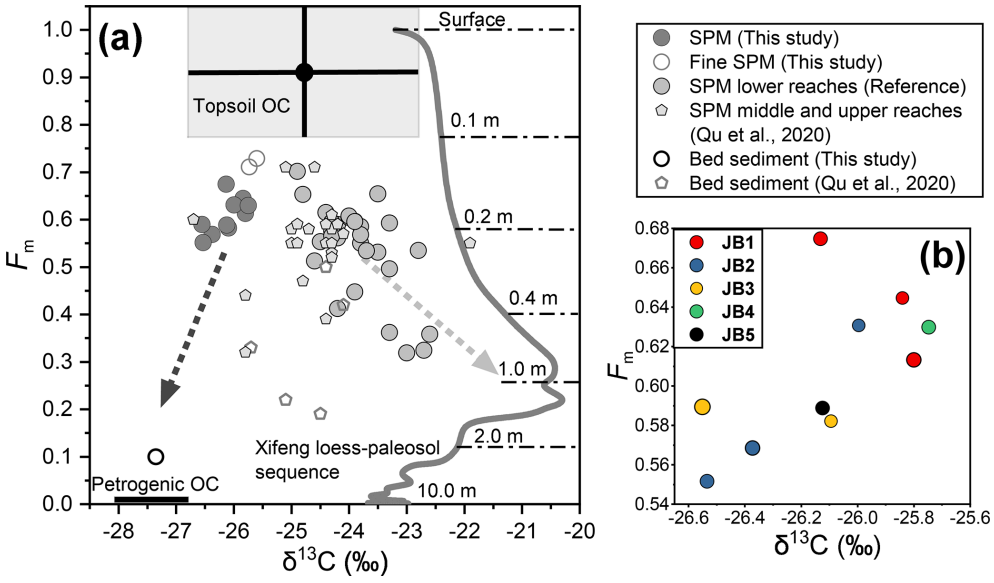


**Figure 5.** **(a)** The $^{14}C$ activity (expressed as $F_m$) vs. $\delta^{13}C$ for a compilation of POC data collected over the 2011–2016 period in the lower Huanghe, including samples from this study and previous studies at Huayuankou, Lijin, and Kenli (Hu et al., 2015; Tao et al., 2015; Yu et al., 2019a; and Ge et al., 2020); SPM and bed sediment (BS) collected by Qu et al. (2020) at Toudaoguai (most downstream location of the upper reaches) and Longmen in the middle reaches (Table S1). The grey curve corresponds to $\delta^{13}C_{org}$ of the top 10 m of the Xifeng loess–paleosol (Ning et al., 2006), and the corresponding $F_m$ was calculated from $^{10}Be$-derived ages following "$Age = -8033 \cdot \ln(F_m)$". The soil depth is marked above the dot-dash line (Zhou et al., 2010). Topsoil OC represents OC from the upper 10 cm of the loess–paleosol sequence with standard deviation marked with black lines. **(b)** The $^{14}C$ activity (expressed as $F_m$) vs. $\delta^{13}C$ diagram for the Huanghe sediment samples collected in this study at the Luokou cross-section. Symbol size increases with sampling depth in the water column.

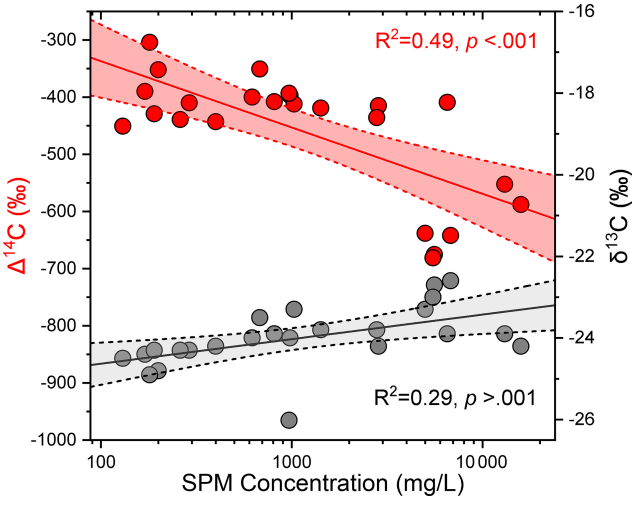


**Figure 6.** The $^{14}C$ activity (expressed as $F_m$; red circles) and $\delta^{13}C$ (grey circles) of POC vs. SPM concentration for surface samples from the Huanghe collected from 2011 to 2016 (average SPM concentration of surface samples in this study and from Hu et al., 2015, Tao et al., 2015, Yu et al., 2019a, and Ge et al., 2020). These paired dual carbon isotope data correspond to the group "SPM lower reaches" in Fig. 5. Straight lines correspond to best-fit logarithmic curves, and shaded areas represent the 95 % confidence interval.

and isotopic signature of POC in the lower Huanghe. Erosion of loess–paleosol can also explain the decreasing POC % with increasing SPM concentration at different sites of the main channel (Ran et al., 2013; Qu et al., 2020), the negative relationship between SPM concentration and corresponding POC $F_m$ at Luokou ($R^2 = 0.49$, $p < 0.001$, Fig. 6), and the low POC loading of the Huanghe (Sect. 5.1.1), as the deep horizons of the loess–paleosol sequences are OC poor and mostly host OC that is highly degraded and refractory (Liu et al., 2012; Wang et al., 2013; Cheng et al., 2020). However, the slight increase in POC $\delta^{13}C$ with increasing SPM concentration ($R^2 = 0.29$, $p > 0.001$) might indicate a significant supply of soil OC from loess–paleosol shallower depth, as inferred from the $\delta^{13}C$ variation within the Xifeng loess–paleosol sequence (Fig. 5a).

The $N/C_{org}$ ratio provides additional evidence for the significant contribution of loess–paleosol material to Huanghe POC (Fig. S6 in the Supplement). Indeed, the $N/C_{org}$ ratios of SPM collected in the lower reaches ranges from 0.10 to 0.23 (this study, Ran et al., 2013; Yu et al., 2019a), whereas topsoils of the CLP are characterized by $N/C_{org}$ lower than 0.14 (Liu and Liu, 2017) and sedimentary rocks typically have very low $N/C_{org}$ (Hilton et al., 2015). Soil OC input from the North China Plain is also unlikely given its $N/C_{org}$ of 0.10–0.13 (Shi et al., 2016). Therefore, all these possible sources cannot explain the high $N/C_{org}$ sig-

natures of riverine SPM. In addition, the high turbidity of the Huanghe ($> 600\,mg\,L^{-1}$) during the sampling season is likely to inhibit in situ primary production ($N/C_{org} > 0.13$) (Zhang et al., 2013; Hu et al., 2015). As a result, only soil OC from deep loess–paleosol horizons appears as a plausible supplier to downstream Huanghe POC, given the high $N/C_{org}$ ratios previously reported for various loess–paleosol sequences (Fig. S6, Ning et al., 2006).

Geomorphic processes in the CLP region support the erosion of deep soil horizons. There, gully erosion is thought to be responsible for more than 80 % of the total sediment yield in the CLP (He et al., 2006; Li et al., 2022). Gullies are densely distributed and cover about 42 % of the total area of the CLP and up to 60 % in hilly regions (Huang and Ren, 2006; He et al., 2006). Nowadays, the well-developed gully geomorphic system of the CLP is characterized by gullies with a depth of about 10 m on average and represents the most active vertical and regressive erosion of loess (Huang and Ren, 2006). This incision process erodes all types of unconsolidated materials, including the loess–paleosol sequence, underlaying red clays, and colluvial deposits in the form of creeps, falls, and slides in the watershed (Zhu, 2012). From 1925 to 1981, the erosion rate of the CLP was $6318\,t\,km^{-2}\,yr^{-1}$, compared to $10\,770\,t\,km^{-2}\,yr^{-1}$ in the hilly and gully plateau (Li et al., 2022). While the CLP's erosion rate dropped to $3476\,t\,km^{-2}\,yr^{-1}$ between 1982 and 2016, the rate in the hilly and gully plateau remained significantly high at $6146.5\,t\,km^{-2}\,yr^{-1}$ (Li et al., 2022). All these observations suggest that gully erosion can strongly impact the composition of riverine POC. As gully erosion is sensitive to climate change and anthropogenic activities, soil dynamics in the Huanghe basin have been altered since the mid-Holocene (He et al., 2006; Li et al., 2022). Notably, the strengthening of the East Asian Monsoon in coming decades (Li et al., 2022; Xue et al., 2023) could potentially enhance this process. However, in recent years, soil and water conservation and environmental rehabilitation campaigns (Wang et al., 2007) largely contributed to a reduction in SPM export by the Huanghe with a transfer to the estuary of 10.6 Mt in 2016, which is an order of magnitude lower than the annual sediment flux measured in 2013 (172.8 Mt) and 2 orders or magnitude lower compared to the flux of the 1950s (ca. 1340 Mt; S. Wang et al., 2016). This sediment load reduction is consistent with the weakened erosion rate observed in the CLP, such modifications should thus have drastically inhibited the OC mobilization from the CLP and the POC export by the Huanghe.

#### 5.2.2 POC source determination and end-member apportionment

Considering the SPM geochemistry and the basin characteristics, three terrestrial sources can be identified as necessary to form the composition of the Huanghe POC at the Luokou cross-section. As discussed in Sect. 5.2.1 and shown in Fig. 5a, two of these sources are (i) topsoil-derived OC ($OC_{ts}$) and (ii) OC from deeper horizons of the loess–paleosol sequence ($OC_{lps}$) excluding topsoil. In addition, at the Luokou cross-section, bed OC shows lower $F_m$ and $\delta^{13}C$ values compared to that of SPM, suggesting a significant contribution of (iii) rock-derived OC from erosion in the middle reaches ($OC_{petro}$).

**Table 2.** Summary of $\delta^{13}C$ and $\Delta^{14}C$ of source end-members for POC in the Huanghe.

| End-member | $\delta^{13}C$ | $\Delta^{14}C$ |
|---|---|---|
| $OC_{ts}$ | $-24.8 \pm 1.9$ ‰ | $-90 \pm 130$ ‰ |
| $OC_{lps}$ | $-22.7 \pm 1.0$ ‰ | $-610 \pm 390$ ‰ |
| $OC_{petro}$ | $-28.1 \pm 1.5$ ‰ | $-1000$ ‰ |

We adopted a Bayesian Monte Carlo model to reconstruct source apportionment based on the mass balance of carbon isotopes ($\delta^{13}C$ and $\Delta^{14}C$) of our three defined end-members (Sect. 3.3, Table 2, Appendix A). The mixing space showing the geometric area between three end-members is shown in Fig. S7 in the Supplement. Modeling results are shown in Fig. 7 as relative contributions (Fig. 7a) and weight percentage (Fig. 7b) of $OC_{ts}$, $OC_{lps}$, and $OC_{petro}$ (Table S2 in the Supplement). The contribution of $OC_{petro}$ to total Huanghe POC at Luokou varies between 10.1 % and 13.9 % in the cross-section, which is higher than the contribution calculated for in the two fine SPM samples (avg. $9.1 \pm 0.3$ %) and much smaller than for the bed sediment sample ($72.2 \pm 10$ %). The inferred $OC_{petro}$ concentration in the sediment is remarkably uniform in the cross-section, representing 0.04 % of SPM (Fig. 7b). This result is consistent with the OC contents of midstream sedimentary rocks at $0.09 \pm 0.08$ % (Qu et al., 2020). In addition, these findings imply that $OC_{petro}$ concentration does not depend on particle size and confirm previous findings of $OC_{petro}$ being present in a range of clastic particles or as discrete particles (Galy et al., 2008a; Bouchez et al., 2014). In other words, the rock-derived OC has a relatively invariant contribution with depth (Galy et al., 2008a; Bouchez et al., 2014), meaning that biospheric OC exerts a first-order control on POC content and isotopic variations throughout the cross-section.

At the study cross-section, $OC_{ts}$ and $OC_{lps}$ contribute 46.6 %–55.4 % and 34.5 %–39.5 % to the total POC, respectively (Fig. 7a). The sum of these two components can be considered $OC_{bio}$, which is $88.0 \pm 1.3$ %. The corresponding $OC_{bio}$ content of sediment is quite variable, ranging from 0.25 % (sample JB 2-3) to 0.40 % (sample JB 1-2) and generally decreases from the river surface to the bottom. Given the rather invariant $OC_{petro}$ concentration in the sediment, there are thus marked heterogeneities of POC provenance in the cross-section. For instance, POC transported close to the right bank and in the finer SPM samples show a higher contribution from $OC_{bio}$. From the knowledge of the rela-

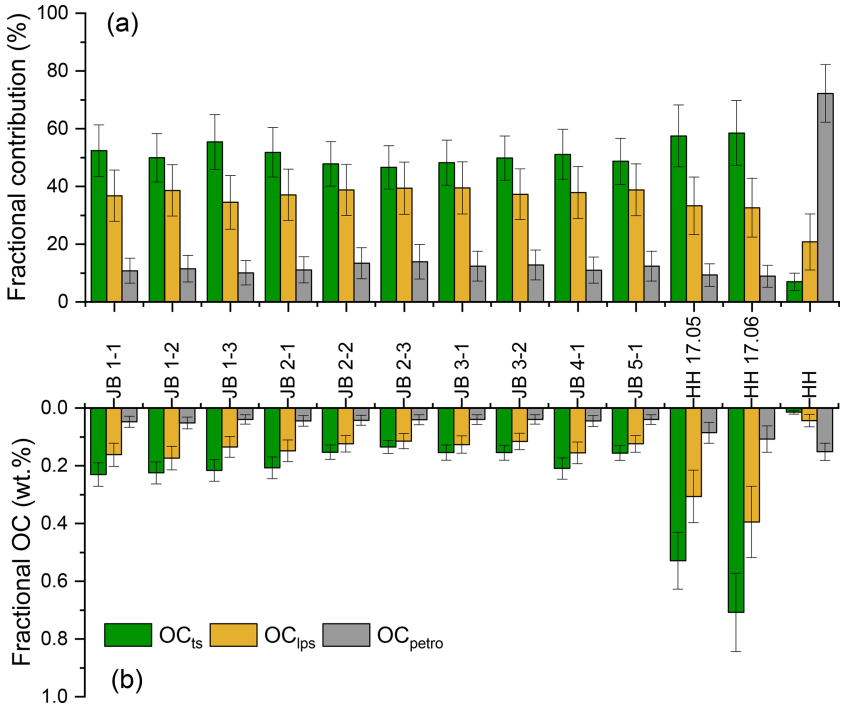


**Figure 7.** **(a)** Relative contributions of the three different sources of Huanghe POC. **(b)** Fractional OC weight percentage Huanghe POC at the Luokou cross-section, as inferred from a mixing model. $OC_{ts}$ is the topsoil-derived OC, $OC_{lps}$ represents the loess–paleosol sequence OC excluding topsoil, and $OC_{petro}$ is the rock-derived OC eroded from the Huanghe middle reaches.

tive contributions of $OC_{ts}$ and $OC_{lps}$ and their corresponding $^{14}C$ activity, the $F_m$ values for the bulk $OC_{bio}$ can be estimated based on mass balance. The modeled radiocarbon activity of $OC_{bio}$ varies from 0.64 to 0.75, corresponding to 3570 to 2300 $^{14}C$ years. In summary, our results support the first-order control of $OC_{bio}$ abundance on POC content and age in the Huanghe.

Applying the same mixing model to previously published Huanghe POC data (2011–2016, Table S1) shows (i) dominance of the $OC_{bio}$ contribution to POC, (ii) variable relative mixing proportions of $OC_{ts}$ and $OC_{lps}$, and (iii) a wide range of $^{14}C$ ages for $OC_{bio}$ (from 1779 to 8325 years). In particular, $OC_{ts}$ and $OC_{lps}$ contributed 28 %–35 % and 53 %–63 % to POC collected in 2013 (Hu et al., 2015), leading to 75 %–89 % of $OC_{bio}$, respectively. Yu et al. (2019a) estimated that $OC_{bio}$ contributed 63 %–81 % to the lower Huanghe POC (2015–2016) using a different mixing model. Using their data in our mixing model results in a higher $OC_{bio}$ contribution of 88 %–91 %, consisting of 43 %–55 % for $OC_{ts}$ and 36 %–46 % for $OC_{lps}$. The small difference in source contribution mainly results from the fact that old $OC_{bio}$ from loess–paleosol sequences was not considered in Yu et al. (2019a) and from the different isotopic signatures chosen for the POC end-members. However, both estimates ignore the possible presence of rock-derived OC in soils. In any case, our results suggest that the Huanghe transports more $OC_{bio}$-derived POC than previously thought with more aged soil-derived OC.

It is worth noticing that these calculations suggest that the $OC_{lps}$ fraction in the Huanghe was significantly higher in 2013 than in 2016. As most Huanghe sediments are derived from the CLP, higher physical erosion in the CLP should enhance supply of aged, refractory $OC_{bio}$ to the river system. Consequently, the decrease in sediment supply from the CLP initiated a few decades ago (S. Wang et al., 2016), which is likely to continue in the future, will probably lead to a reduction in the contribution of $OC_{lps}$ to total POC export from the Huanghe. This might have an impact on the burial efficiency of riverine POC on the continental margins, as $OC_{ts}$ is more labile than $OC_{lps}$ and thus more prone to the remineralization process before burial. Moreover, decreasing erosion rate in the Huanghe basin will lead to decreasing sediment accumulation rate in the estuary, which potentially favors the oxidation of all POC components before burial (Blair and Aller, 2012). The timescale over which such effect could take place is yet unknown, as anthropogenic intervention is the primary reason for the sediment yield reduction, through afforestation and soil and water conservation measures in the CLP and reservoir operation in the middle reaches of the Huanghe. However, it is plausible that in response to decreased terrestrial physical erosion on the Loess Plateau over at least decadal timescales, an increased proportion of Huanghe POC will be oxidized before burial in the ocean, thereby leading to

a weakened preservation efficiency for the terrestrial eroded POC.

### 5.3 POC export by the Huanghe

In the Huanghe, POC content varies both vertically and laterally throughout the cross-section (Fig. 2). This spatial variability of both physical and chemical SPM characteristics must be considered when estimating integrated instantaneous POC concentration and flux (Sect. 3.4).

We calculate that (Sect. S1) at the sampling time (July 2016), the Huanghe at Luokou transported $1075\,\mathrm{kg\,s^{-1}}$ of SPM for a water discharge of $731\,\mathrm{m^3\,s^{-1}}$, such that the spatially integrated SPM concentration over the cross-section ($SPM_{int}$) was $1472\,\mathrm{mg\,L^{-1}}$, a value relatively close to the straightforward average concentration of our 10 samples ($1286\,\mathrm{mg\,L^{-1}}$). The Luokou gauging station records a monthly SPM load of $1826\,\mathrm{kg\,s^{-1}}$ in July 2016, and a daily average SPM load of $1096\,\mathrm{kg\,s^{-1}}$ for a daily average water discharge of $643\,\mathrm{m^3\,s^{-1}}$ on the 16 and 17 July 2016 (the method used is as follows: three water samples collected at 0.5 m below the channel surface across the transect profile; data available at http://www.yrcc.gov.cn, last access: 15 November 2021). Even though the latter estimate neglects the vertical heterogeneity within this relatively shallow river ($< 5.0$ m), estimates give similar results.

We further obtain an instantaneous POC flux of $3.69\,\mathrm{kg\,s^{-1}}$, corresponding to a cross-section-integrated average POC content ($POC_{int}$ %) of 0.34 % when dividing this instantaneous POC flux by the instantaneous SPM load. Given the relatively homogenous distribution of $OC_{petro}$, the instantaneous flux of $OC_{petro}$ was calculated by multiplying the average $OC_{petro}$ content by the instantaneous cross-section-integrated SPM flux, yielding $0.44 \pm 0.18\,\mathrm{kg\,s^{-1}}$. The instantaneous $OC_{bio}$ flux was then calculated by subtracting the instantaneous flux of $OC_{petro}$ from the instantaneous POC flux, yielding $3.25 \pm 0.20\,\mathrm{kg\,s^{-1}}$. Assuming that our SPM samples are representative in terms of POC content exported in July 2016, and taking the SPM flux of the gauging station for July, then the estimated fluxes of POC, $OC_{bio}$, and $OC_{petro}$ for the flood period of July 2016 are 6.1, 5.4, and $0.7\,\mathrm{kg\,s^{-1}}$, respectively. Taking $POC_{int}$ content for estimating the annual POC flux yields, a value of $1.1\,\mathrm{kg\,s^{-1}}$ consisting of 1.0 and $0.1\,\mathrm{kg\,s^{-1}}$ is found for $OC_{bio}$ and $OC_{petro}$ fluxes, respectively. Note that these numbers are lower-bound estimates because POC content in Huanghe SPM collected during flood periods is generally the lowest (Ran et al., 2013). Taking the highest POC content, 0.75 % reported in the lower Huanghe in 2016 (Yu et al., 2019a), the estimated annual POC flux is $2.4\,\mathrm{kg\,s^{-1}}$.

The above numbers present a sharp decrease compared to the estimated POC and $OC_{bio}$ fluxes transported by the Huanghe over the period 2008 to 2013. Galy et al. (2015) estimated an $OC_{petro}$ flux of $1.9\,\mathrm{kg\,s^{-1}}$ and an $OC_{bio}$ flux of $11.4\,\mathrm{kg\,s^{-1}}$ from 2008 to 2012 (SPM flux: $3655\,\mathrm{kg\,s^{-1}}$, YRCC 2016), while Tao et al. (2018) reported an $OC_{petro}$ flux of $5.8\,\mathrm{kg\,s^{-1}}$ and a similar $OC_{bio}$ flux of $12.6\,\mathrm{kg\,s^{-1}}$ from June 2012 to May 2013 (SPM flux: $5723\,\mathrm{kg\,s^{-1}}$, YRCC 2016).

We first note that previous estimates of POC flux in the Huanghe might be biased as these estimates neglect the variability over the cross-section (e.g., Hu et al., 2015; Ran et al., 2013; Tao et al., 2015); SPM samples analyzed so far for the Huanghe were generally collected within the first 0.5 m below the surface, meaning that previous POC estimates did not consider the observed vertical and lateral POC heterogeneities and have thus misestimated POC sources and fluxes. Those estimates were calculated by multiplying an individual surface POC content by the corresponding monthly or weekly suspended sediment load, as provided by hydrological stations. Such estimates can be problematic because POC content in SPM generally decreases from top to bottom (Fig. 2), resulting in biased surface-based estimates of fluxes (Bouchez et al., 2014). Using our cross-section data, we can estimate the bias in POC flux estimates when a single sample is used for such flux estimates by multiplying depth-integrated sediment flux by the POC content of each sample. Such calculation shows different POC fluxes ranging from $-15$ % to $+30$ % compared to the depth-integrated estimate, which is mostly influenced by the variable POC content. Considering SPM collected at the channel surface, POC flux estimates using samples JB 1-1 and JB 2-1 are 28 % and 15 % higher, respectively, and are 6 % and 5 % lower using samples JB 3-1 and JB 5-1, respectively, than the depth-integrated estimate. This simple sensitivity analysis shows that channel surface sampling of SPM alone does not necessarily result in an overestimation of POC flux because of lateral heterogeneity, even though the POC content of SPM is generally higher at the surface than at the bottom (Fig. 2). Consequently, and although accurate estimation of POC fluxes requires grain size variations to be accounted for, the corresponding bias cannot explain the large difference between our estimates of Huanghe POC export for the year 2016 and previous estimates for preceding years. The SPM flux is $336\,\mathrm{kg\,s^{-1}}$ in 2016 and $762\,\mathrm{kg\,s^{-1}}$ over the period 2014 to 2016, which is an order of magnitude lower than values reported from 2008 to 2013 (YRCC 2016). The dramatic decrease in sediment load of the Huanghe (S. Wang et al., 2016) has most likely exerted a first-order control on the reduction in POC export from the Huanghe river system and will probably continue to do so in the near future.

In the lower Huanghe, the POC content is very low and has small variance among different size fractions (Ge et al., 2020), such that the POC flux is controlled by the SPM flux. In particular, it is worth noting that the Huanghe displays strong density stratification effects compared to other rivers (Moodie et al., 2022), with near-bed flow dominating the transport of SPM. In order to appraise how spatial and temporal variability in SPM flux could influence POC export, "local" POC loads can be calculated throughout the

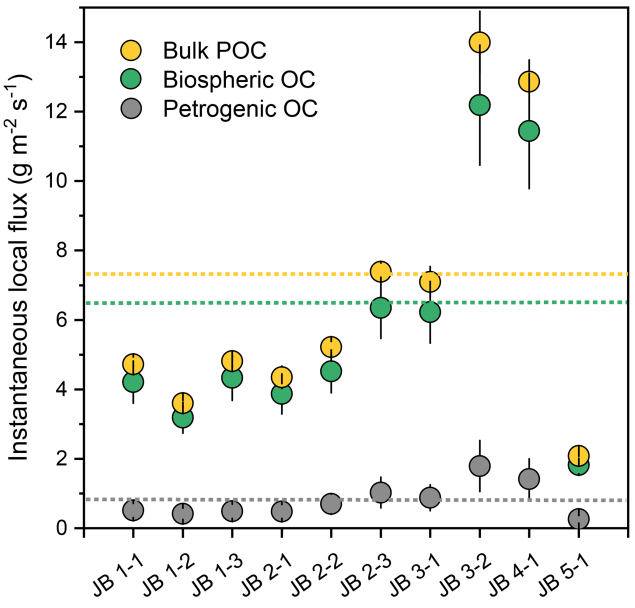


**Figure 8.** Estimates of instantaneous "local" fluxes of Huanghe bulk POC, $OC_{bio}$, and $OC_{petro}$, calculated for each sample of the Luokou cross-section. The three dotted lines marked in orange, green, and grey represent the corresponding instantaneous, cross-section-integrated fluxes. The error bar represents 1 standard deviation.

cross-section using the local water velocity, SPM concentration, and POC content (Fig. 8). In general, in the lower Huanghe more POC is transported near the riverbed and above shallower bathymetry on the left side of the channel (except for profile JB 5). For instance, there is a nearly two-fold increase in POC export from the surface to the bottom for the JB 2 and JB 3 profiles. The maximum local bulk POC ($14.0\,g\,C\,m^{-2}\,s^{-1}$), $OC_{bio}$ ($12.2\,g\,C\,m^{-2}\,s^{-1}$), and $OC_{petro}$ export ($1.8\,g\,C\,m^{-2}\,s^{-1}$) are of sample JB 3-2, representing over 6 times the size of the corresponding minimum value (sample JB 5-1). This spatial pattern of POC load is almost the reverse of the POC% variation over the cross-section, again stressing the importance of sediment river dynamics in POC delivery. From these considerations, it could be anticipated that during the low-water season, when water velocity is slower, near-bottom Huanghe SPM is deposited on the channel bed, withdrawing a significant fraction of the POC export, as shown in other large rivers (Ke et al., 2022). This topic should be further examined in future research, in order to systematically investigate the stratification of sediment and associated OC transport dynamics in lowland and high-turbidity fluvial systems.

Interestingly, anthropogenic activities may have antagonistic effects on POC export. Deforestation, agriculture, and mining have considerably enhanced the sediment yield from the CLP since the mid-Holocene (He et al., 2006) while the construction of large dams, soil and water conservation measures, and afforestation have considerably reduced the sediment yield since the 1950s (S. Wang et al., 2016; Wang et al., 2007; Syvitski et al., 2005). However, the Huanghe exports substantial $OC_{bio}$ and $OC_{petro}$ with a significantly higher burial efficiency (avg. ca. 42 %; Sun et al., 2018) than other large fluvial systems entering passive continental margins, such as the Changjiang, Amazon, and Mississippi rivers (Blair and Aller, 2012). It is reported that aged soil OC is nearly fully preserved in continental margins and that $OC_{petro}$ has a ca. 70 % burial efficiency (Tao et al., 2016). However, the contribution of the Huanghe OC burial to the global C sink is likely to be lower in the future as the consequence of the (i) sharp decrease in SPM and POC export due to weakened physical erosion in the CLP and (ii) reduced sediment accumulation rate favoring OC remineralization in estuaries (Blair and Aller, 2012; Walling and Fang, 2003; Milliman and Farnsworth, 2011; Galy et al., 2015).

## 6 Conclusions

In this contribution, we present the first detailed study of particulate organic carbon (POC) over a complete river cross-section of the Huanghe, providing new perspectives on the transport mode, source, and instantaneous fluxes of POC in this highly turbid large river.

At the scale of a cross-section, physical and chemical properties of SPM are heterogeneous both vertically and laterally, a feature that is mainly controlled by bathymetry and hydrodynamic sorting. Resuspension of bed sediment and local erosion of the right bank together impact the suspended POC composition at the sampled location. This spatial heterogeneity shows that near-bottom SPM plays a dominant role in the delivery of $OC_{bio}$ (topsoil and deep soil OC combined) and $OC_{petro}$. Despite a relatively shallow river channel ($< 5.0$ m) and narrow width ($< 200$ m), we show how the heterogeneity of POC transport over a cross-section needs to be considered in constraining the POC transport mode and estimating POC fluxes.

Despite its millennial age, POC in the Huanghe is dominated by $OC_{bio}$ with a contribution of $88.0 \pm 1.3$ %. $OC_{petro}$ content in SPM is relatively homogeneous (0.04 %–0.05 %) over the cross-section, indicating that the variability in bulk POC age is mainly controlled by the variability in $OC_{bio}$ content, especially in the finest SPM fraction. $OC_{bio}$ ages deduced from the application of a mixing model to previously published data (record period 2011–2016) are highly variable, ranging from 1779 to 8325 $^{14}C$ years. We interpret this feature as resulting from the erosion of deep horizons by gully systems in the loess–paleosol sequences containing $^{14}C$-dead $OC_{bio}$. Enhanced erosion of deep loess–paleosol horizons mobilizes aged and refractory OC to the ocean, with high burial efficiency on the passive margin. The erosion of loess–paleosol horizons is thus an efficient process of $CO_2$ burial. However, the construction of large dams has drastically affected the sediment load of the Huanghe sys-

tem and retains substantial quantities of sediments that were previously exported to the ocean. Future work is needed to further quantify how these anthropogenic modifications alter POC composition and transport by conducting comprehensive cross-section sampling campaigns over extended time series upstream and downstream from dams.

## Appendix A

Fluvial POC delivered in the Huanghe POC could originate from three terrestrial sources (Table 2). As topsoil typically contains recently photosynthesized $OC_{bio}$, we used a $\delta^{13}C$ value of $-24.8 \pm 1.9$ ‰ ($n = 166$) according to the subsurface soil OC values measured across the Huanghe basin (Rao et al., 2017). Over the sampled cross-section, the depleted $^{13}C$ values indicate the dominant and almost exclusive input of C3 plant-derived material to the Huanghe POC in the lower reaches. Based on $^{14}C$ (Liu et al., 2012) and $^{10}Be$ (Zhou et al., 2010) dating of $< 10$ cm deep soil horizons in the Huanghe Basin, the average age of topsoil was chosen as being younger than 2000 years (i.e., $\Delta^{14}C > -220$ ‰). As the topsoil end-member includes modern biospheric material ($\Delta^{14}C$ around 40 ‰, Hua et al., 2013), we assigned a $\Delta^{14}C$ value of $-90 \pm 130$ ‰ ($F_m = 0.91 \pm 0.13$). This range also includes the range of $\Delta^{14}C$ values of pre-aged soil OC indicated by the long-chain n-$C_{24+26+28}$ alkanols of the Huanghe POC reported by Tao et al. (2015) and Yu et al. (2019a). Their results show consistent POC $\Delta^{14}C$ values in the lower reaches of $-204 \pm 20$ ‰ ($F_m = 0.80 \pm 0.03$, $n = 7$) from June 2015 to May 2016 and $-219 \pm 33$ ‰ ($F_m = 0.79 \pm 0.04$, $n = 4$) at Kenli and of $-198 \pm 15$ ‰ ($F_m = 0.81 \pm 0.02$, $n = 6$) from June 2015 to April 2016 at Huayuankou (Tao et al., 2015; Yu et al., 2019a).

The second end-member should be characterized by aged and refractory OC from the loess–paleosol sequence excluding topsoil (upper 10 m) of the CLP. Radiocarbon dating has an upper age limit of around 50 000 years, i.e., the age above which $F_m$ is equal to 0. However, radiocarbon-free OC spanning from 50 000 to 100 000 years must still be considered as $OC_{bio}$ in the long-term carbon cycle. Here, we name this ignored OC as the "dormant" OC, without which the $OC_{bio}$ (i.e., less than 100 000 years old) would be underestimated to some extent because the radiocarbon-free OC would be misinterpreted as having a petrogenic origin. To consider this "dormant" OC, $\delta^{13}C$ values of $-22.7 \pm 1.0$ ‰ ($n = 34$, Ning et al., 2006) and $\Delta^{14}C$ values of $-610 \pm 390$ ‰ ($F_m$, $0.39 \pm 0.39$) were adopted based on an average of values over the whole loess–paleosol sequence. Although radiocarbon-free (i.e., older than 100 000 years) OC overlaps with this end-member, such old soil organic carbon is probably not mobilized as modern gully erosion mainly concerns the upper 10 m of the loess–paleosol sequences, where soil $OC_{bio}$ is assumed to be significantly younger comparatively (Fig. 5).

Rock-derived OC from the QTP and the CLP, as well as kerogen from oil and gas fields from the Ordos Basin, were all considered to be possible contributors to the $OC_{petro}$ end-member. The $\delta^{13}C$ of $OC_{petro}$ greatly varies between the QTP ($-21.2 \pm 1.2$ ‰, $n = 11$, Liu et al., 2007) and the CLP ($-26.8 \pm 0.5$ ‰, $n = 8$, Qu et al., 2020). However, most of the sediments eroded from the QTP are not transferred to the lower reaches as they remain trapped in the CLP and the western Mu Us desert (Nie et al., 2015; Licht et al., 2016; Pan et al., 2016). In addition, the construction of large dams in the upper reaches has considerably reduced the transfer of solid materials downstream (Wang et al., 2007). Therefore, rock-derived OC inherited from the denudation of the QTP region is not further considered. Kerogen from the oil and gas fields of the Ordos Basin in the CLP region (Fig. 1) has $\delta^{13}C$ values of $-29.2 \pm 0.9$ ‰ ($n = 10$, Guo et al., 2014). Taking these constraints together, we consider a $\delta^{13}C$ value of $-28.1 \pm 1.5$ ‰ ($n = 18$) for the $OC_{petro}$ end-member, and a $\Delta^{14}C$ value of $-1000$ ‰ ($F_m = 0$) by definition.

## Highlights

- Bank erosion in lower Huanghe provides recent organic carbon to fluvial transport, altering the particulate organic carbon transport over a river channel cross-section.
- Erosion of deep soil horizons of the loess–paleosol sequence contributes radiocarbon-dead organic carbon from the biosphere to the Huanghe.
- Channel-bottom transport in the Huanghe is the primary process of exporting fluvial particulate organic carbon to the estuary.

**Data availability.** All datasets are included in the paper (Table 1) and the Supplement.

**Supplement.** The supplement related to this article is available online at: https://doi.org/10.5194/esurf-12-347-2024-supplement.

**Author contributions.** DC, JB, CQ, and YK conceptualized the study. DC, JB, YK, MM, and BC determined the methodology. HC and JC collected the sediment samples. YK, MM, and AN assisted with elemental and isotopic carbon analysis. DC and CQ supervised the work. YK performed data analysis and wrote the original draft, and all authors contributed to the review and editing of the paper.

**Competing interests.** The contact author has declared that none of the authors has any competing interests.

**Acknowledgements.** We thank Yulong Liu and Shengliu Yuan for their help during sampling and filtering. We also thank François Thil and Nadine Tissenerat for invaluable help when running the ECHoMICADAS and Pierre Barré for the use of the Beckman Coulter's LS 13 320 for particle size analysis at École Normale supérieure.

**Financial support.** This research has been supported by the Agence Nationale de la Recherche (grant no. ANR-15-CE01-0012), the National Natural Science Foundation of China (grant no. 41561134017), the National Natural Science Foundation of China (grant no. 41625012), and the China Scholarship Council (grant no. 201706180008).

**Review statement.** This paper was edited by Robert Hilton and reviewed by Melissa Schwab and one anonymous referee.

## References

Baronas, J. J., Stevenson, E. I., Hackney, C. R., Darby, S. E., Bickle, M. J., Hilton, R. G., Larkin, C. S., Parsons, D. R., Myo Khaing, A., and Tipper, E. T.: Integrating Suspended Sediment Flux in Large Alluvial River Channels: Application of a Synoptic Rouse-Based Model to the Irrawaddy and Salween Rivers, J. Geophys. Res.-Earth, 125, e2020JF005554, https://doi.org/10.1029/2020jf005554, 2020.

Bianchi, T. S.: The role of terrestrially derived organic carbon in the coastal ocean: A changing paradigm and the priming effect, P. Natl. Acad. Sci. USA, 108, 19473–19481, https://doi.org/10.1073/pnas.1017982108, 2011.

Bird, A., Stevens, T., Rittner, M., Vermeesch, P., Carter, A., Andò, S., Garzanti, E., Lu, H., Nie, J., Zeng, L., Zhang, H., and Xu, Z.: Quaternary dust source variation across the Chinese Loess Plateau, Palaeogeogr. Palaeocl., 435, 254–264, https://doi.org/10.1016/j.palaeo.2015.06.024, 2015.

Blair, N. E. and Aller, R. C.: The Fate of Terrestrial Organic Carbon in the Marine Environment, Annu. Rev. Mar. Sci., 4, 401–423, https://doi.org/10.1146/annurev-marine-120709-142717, 2012.

Blair, N. E., Leithold, E. L., Brackley, H., Trustrum, N., Page, M., and Childress, L.: Terrestrial sources and export of particulate organic carbon in the Waipaoa sedimentary system: Problems, progress and processes, Mar. Geol., 270, 108–118, https://doi.org/10.1016/j.margeo.2009.10.016, 2010.

Bouchez, J., Beyssac, O., Galy, V., Gaillardet, J., France-Lanord, C., Maurice, L., and Moreira-Turcq, P.: Oxidation of petrogenic organic carbon in the Amazon floodplain as a source of atmospheric $CO_2$, Geology, 38, 255–258, https://doi.org/10.1130/G30608.1, 2010.

Bouchez, J., Gaillardet, J., France-Lanord, C., Maurice, L., and Dutra-Maia, P.: Grain size control of river suspended sediment geochemistry: Clues from Amazon River depth profiles, Geochem. Geophy. Geosy., 12, Q03008, https://doi.org/10.1029/2010gc003380, 2011a.

Bouchez, J., Lupker, M., Gaillardet, J., France-Lanord, C., and Maurice, L.: How important is it to integrate riverine suspended sediment chemical composition with depth? Clues from Amazon River depth-profiles, Geochim. Cosmochim. Ac., 75, 6955–6970, https://doi.org/10.1016/j.gca.2011.08.038, 2011b.

Bouchez, J., Galy, V., Hilton, R. G., Gaillardet, J., Moreira-Turcq, P., Pérez, M. A., France-Lanord, C., and Maurice, L.: Source, transport and fluxes of Amazon River particulate organic carbon: Insights from river sediment depth-profiles, Geochim. Cosmochim. Ac., 133, 280–298, https://doi.org/10.1016/j.gca.2014.02.032, 2014.

Carignan, J., Hild, P., Mevelle, G., Morel, J., and Yeghicheyan, D.: Routine Analyses of Trace Elements in Geological Samples using Flow Injection and Low Pressure On-Line Liquid Chromatography Coupled to ICP-MS: A Study of Geochemical Reference Materials BR, DR-N, UB-N, AN-G and GH, Geostandard. Newslett., 25, 187–198, https://doi.org/10.1111/j.1751-908X.2001.tb00595.x, 2001.

Cauwet, G. and Mackenzie, F. T.: Carbon inputs and distribution in estuaries of turbid rivers: the Yang Tze and Yellow rivers (China), Mar. Chem., 43, 235–246, https://doi.org/10.1016/0304-4203(93)90229-h, 1993.

Cheng, P., Burr, G. S., Zhou, W., Chen, N., Hou, Y., Du, H., Fu, Y., and Lu, X.: The deficiency of organic matter $^{14}C$ dating in Chinese Loess-paleosol sample, Quat. Geochronol., 56, 101051, https://doi.org/10.1016/j.quageo.2019.101051, 2020.

Curry, K. J., Bennett, R. H., Mayer, L. M., Curry, A., Abril, M., Biesiot, P. M., and Hulbert, M. H.: Direct visualization of clay microfabric signatures driving organic matter preservation in fine-grained sediment, Geochim. Cosmochim. Ac., 71, 1709–1720, https://doi.org/10.1016/j.gca.2007.01.009, 2007.

Feng, X., Feakins, S. J., Liu, Z., Ponton, C., Wang, R. Z., Karkabi, E., Galy, V., Berelson, W. M., Nottingham, A. T., Meir, P., and West, A. J.: Source to sink: Evolution of lignin composition in the Madre de Dios River system with connection to the Amazon basin and offshore, J. Geophys. Res.-Biogeo., 121, 1316–1338, https://doi.org/10.1002/2016JG003323, 2016.

Freymond, C. V., Lupker, M., Peterse, F., Haghipour, N., Wacker, L., Filip, F., Giosan, L., and Eglinton, T. I.: Constraining Instantaneous Fluxes and Integrated Compositions of Fluvially Discharged Organic Matter, Geochem. Geophy. Geosy. 19, 2453–2462, https://doi.org/10.1029/2018gc007539, 2018.

Galy, V. and Eglinton, T.: Protracted storage of biospheric carbon in the Ganges–Brahmaputra basin, Nat. Geosci., 4, 843–847, https://doi.org/10.1038/ngeo1293, 2011.

Galy, V., France-Lanord, C., Beyssac, O., Faure, P., Kudrass, H., and Palhol, F.: Efficient organic carbon burial in the Bengal fan sustained by the Himalayan erosional system, Nature, 450, 407–10, https://doi.org/10.1038/nature06273, 2007.

Galy, V., Beyssac, O., France-Lanord, C., and Eglinton, T.: Recycling of graphite during Himalayan erosion: a geological stabilization of carbon in the crust, Science, 322, 943–5, https://doi.org/10.1126/science.1161408, 2008a.

Galy, V., France-Lanord, C., and Lartiges, B.: Loading and fate of particulate organic carbon from the Himalaya to the Ganga–Brahmaputra delta, Geochim. Cosmochim. Ac., 72, 1767–1787, https://doi.org/10.1016/j.gca.2008.01.027, 2008b.

Galy, V., Peucker-Ehrenbrink, B., and Eglinton, T.: Global carbon export from the terrestrial biosphere controlled by erosion, Nature, 521, 204–7, https://doi.org/10.1038/nature14400, 2015.

Garcia, M. (Ed.): Sedimentation Engineering, American Society of Civil Engineers, 21–163 https://doi.org/10.1061/9780784408148, 2008.

Garzanti, E., Andò, S., France-Lanord, C., Vezzoli, G., Censi, P., Galy, V., and Najman, Y.: Mineralogical and chemical variability of fluvial sediments: 1. Bedload sand (Ganga–Brahmaputra, Bangladesh), Earth Planet. Sci. Lett., 299, 368–381, https://doi.org/10.1016/j.epsl.2010.09.017, 2010.

Ge, T., Xue, Y., Jiang, X., Zou, L., and Wang, X.: Sources and radiocarbon ages of organic carbon in different grain size fractions of Yellow River-transported particles and coastal sediments, Chem. Geol., 534, 119452, https://doi.org/10.1016/j.chemgeo.2019.119452, 2020.

Guo, H., Jia, W., Peng, P., Lei, Y., Luo, X., Cheng, M., Wang, X., Zhang, L., and Jiang, C.: The composition and its impact on the methane sorption of lacustrine shales from the Upper Triassic Yanchang Formation, Ordos Basin, China, Mar. Petrol. Geol., 57, 509–520, https://doi.org/10.1016/j.marpetgeo.2014.05.010, 2014.

Guo, L., Ping, C.-L., and Macdonald, R. W.: Mobilization pathways of organic carbon from permafrost to arctic rivers in a changing climate, Geophys. Res. Lett., 34, L13603, https://doi.org/10.1029/2007GL030689, 2007.

Guo, Z. T., Ruddiman, W. F., Hao, Q. Z., Wu, H. B., Qiao, Y. S., Zhu, R. X., Peng, S. Z., Wei, J. J., Yuan, B. Y., and Liu, T. S.: Onset of Asian desertification by 22 Myr ago inferred from loess deposits in China, Nature, 416, 159–163, https://doi.org/10.1038/416159a, 2002.

Hatté, C., Arnold, M., Dapoigny, A., Daux, V., Delibrias, G., Boisgueheneuc, D. D., Fontugne, M., Gauthier, C., Guillier, M.-T., Jacob, J., Jaudon, M., Kaltnecker, É., Labeyrie, J., Noury, C., Paterne, M., Pierre, M., Phouybanhdyt, B., Poupeau, J.-J., Tannau, J.-F., Thil, F., Tisnérat-Laborde, N., and Valladas, H.: Radiocarbon dating on ECHOMICADAS, LSCE, Gif-Sur-Yvette, France: new and updated chemical procedures, Radiocarbon, 1–16, https://doi.org/10.1017/RDC.2023.46, 2023.

He, X., Tang, K., and Zhang, X.: Soil Erosion Dynamics on the Chinese Loess Plateau in the Last 10,000 Years, mred, 24, 342–347, https://doi.org/10.1659/0276-4741(2004)024[0342:SEDOTC]2.0.CO;2, 2004.

He, X., Zhou, J., Zhang, X., and Tang, K.: Soil erosion response to climatic change and human activity during the Quaternary on the Loess Plateau, China, Reg. Environ. Change, 6, 62–70, https://doi.org/10.1007/s10113-005-0004-7, 2006.

Hilton, R. G., Galy, A., Hovius, N., Horng, M.-J., and Chen, H.: Efficient transport of fossil organic carbon to the ocean by steep mountain rivers: An orogenic carbon sequestration mechanism, Geology, 39, 71–74, https://doi.org/10.1130/g31352.1, 2011.

Hilton, R. G., Gaillardet, J., Calmels, D., and Birck, J.-L.: Geological respiration of a mountain belt revealed by the trace element rhenium, Earth Planet. Sci. Lett., 403, 27–36, https://doi.org/10.1016/j.epsl.2014.06.021, 2014.

Hilton, R. G., Galy, V., Gaillardet, J., Dellinger, M., Bryant, C., O'Regan, M., Grocke, D. R., Coxall, H., Bouchez, J., and Calmels, D.: Erosion of organic carbon in the Arctic as a geological carbon dioxide sink, Nature, 524, 84–7, https://doi.org/10.1038/nature14653, 2015.

Horan, K., Hilton, R. G., Dellinger, M., Tipper, E., Galy, V., Calmels, D., Selby, D., Gaillardet, J., Ottley, C. J., Parsons, D. R., and Burton, K. W.: Carbon dioxide emissions by rock organic carbon oxidation and the net geochemical carbon budget of the Mackenzie River Basin, Am. J. Sci., 319, 473–499, https://doi.org/10.2475/06.2019.02, 2019.

Hu, B., Li, J., Bi, N., Wang, H., Wei, H., Zhao, J., Xie, L., Zou, L., Cui, R., Li, S., Liu, M., and Li, G.: Effect of human-controlled hydrological regime on the source, transport, and flux of particulate organic carbon from the lower Huanghe (Yellow River), Earth Surf. Proc. Land., 40, 1029–1042, https://doi.org/10.1002/esp.3702, 2015.

Hua, Q., Barbetti, M., and Rakowski, A. Z.: Atmospheric Radiocarbon for the Period 1950–2010, Radiocarbon, 55, 2059–2072, https://doi.org/10.2458/azu_js_rc.v55i2.16177, 2013.

Huang, C. C. and Ren, Z.: Fluvial erosion and the formation of gully systems over the Chinese Loess Plateau, WSEAS Transactions on Environment and Development, 2, 141–145, 2006.

Jahn, B., Gallet, S., and Han, J.: Geochemistry of the Xining, Xifeng and Jixian sections, Loess Plateau of China: eolian dust provenance and paleosol evolution during the last 140 ka, Chem. Geol., 178, 71–94, https://doi.org/10.1016/S0009-2541(00)00430-7, 2001.

Ke, Y., Calmels, D., Bouchez, J., and Quantin, C.: MOdern River archivEs of Particulate Organic Carbon: MOREPOC, Earth Syst. Sci. Data, 14, 4743–4755, https://doi.org/10.5194/essd-14-4743-2022, 2022.

Komada, T., Anderson, M. R., and Dorfmeier, C. L.: Carbonate removal from coastal sediments for the determination of organic carbon and its isotopic signatures, $\delta^{13}C$ and $\Delta^{14}C$: comparison of fumigation and direct acidification by hydrochloric acid, Limnology and Oceanography Letters, 6, 254–262, 2008.

Lee, H., Galy, V., Feng, X., Ponton, C., Galy, A., France-Lanord, C., and Feakins, S. J.: Sustained wood burial in the Bengal Fan over the last 19 My, P. Natl. Acad. Sci., 116, 22518–22525, https://doi.org/10.1073/pnas.1913714116, 2019.

Li, G., Wang, X. T., Yang, Z., Mao, C., West, A. J., and Ji, J.: Dam-triggered organic carbon sequestration makes the Changjiang (Yangtze) river basin (China) a significant carbon sink, J. Geophys. Res.-Biogeo., 120, 39–53, https://doi.org/10.1002/2014JG002646, 2015.

Li, P., Chen, J., Zhao, G., Holden, J., Liu, B., Chan, F. K. S., Hu, J., Wu, P., and Mu, X.: Determining the drivers and rates of soil erosion on the Loess Plateau since 1901, Sci. Total Environ., 823, 153674, https://doi.org/10.1016/j.scitotenv.2022.153674, 2022.

Licht, A., Pullen, A., Kapp, P., Abell, J., and Giesler, N.: Eolian cannibalism: Reworked loess and fluvial sediment as the main sources of the Chinese Loess Plateau, Geol. Soc. Am. Bull., 128, 944–956, https://doi.org/10.1130/B31375.1, 2016.

Liu, G., Xu, W., Zhang, Q., and Xia, Z.: Holocene Soil Chronofunctions, Luochuan, Chinese Loess Plateau, in: Radiometric Dating, edited by: Nawrocka, D. M., InTech, Janeza Trdine, Rijeka, Croatia, ISBN 978-953-51-0596-1, 2012.

Liu, J. and Liu, W.: Soil nitrogen isotopic composition of the Xifeng loess-paleosol sequence and its potential for use as a paleoenvironmental proxy, Quatern. Int., 440, 35–41, https://doi.org/10.1016/j.quaint.2016.04.018, 2017.

Liu, W., Yang, H., Ning, Y., and An, Z.: Contribution of inherent organic carbon to the bulk $\delta^{13}C$ signal in loess deposits from the arid western Chinese Loess Plateau, Org. Geochem., 38, 1571–1579, https://doi.org/10.1016/j.orggeochem.2007.05.004, 2007.

Ludwig, W., Probst, J.-L., and Kempe, S.: Predicting the oceanic input of organic carbon by continental erosion, Global Biogeochem. Cy., 10, 23–41, https://doi.org/10.1029/95gb02925, 1996.

Mayorga, E., Aufdenkampe, A. K., Masiello, C. A., Krusche, A. V., Hedges, J. I., Quay, P. D., Richey, J. E., and Brown, T. A.: Young organic matter as a source of carbon dioxide outgassing from Amazonian rivers, Nature, 436, 538–41, https://doi.org/10.1038/nature03880, 2005.

Milliman, J. D. and Farnsworth, K. L.: River discharge to the coastal ocean: a global synthesis, Cambridge University Press, Cambridge, the United Kingdom, ISBN 978-0-521-87987-3, 2011.

Milliman, J. D., Yun-Shan, Q., Mei-E, R., and Saito, Y.: Man's Influence on the Erosion and Transport of Sediment by Asian Rivers: The Yellow River (Huanghe) Example, J. Geol., 95, 751–762, https://doi.org/10.1086/629175, 1987.

Moodie, A. J., Nittrouer, J. A., Ma, H., Carlson, B. N., Wang, Y., Lamb, M. P., and Parker, G.: Suspended Sediment-Induced Stratification Inferred From Concentration and Velocity Profile Measurements in the Lower Yellow River, China, Water Resour. Res., 58, e2020WR027192, https://doi.org/10.1029/2020WR027192, 2022.

Moore, J. W. and Semmens, B. X.: Incorporating uncertainty and prior information into stable isotope mixing models, Ecol. Lett., 11, 470–480, https://doi.org/10.1111/j.1461-0248.2008.01163.x, 2008.

Nie, J., Stevens, T., Rittner, M., Stockli, D., Garzanti, E., Limonta, M., Bird, A., Andò, S., Vermeesch, P., Saylor, J., Lu, H., Breecker, D., Hu, X., Liu, S., Resentini, A., Vezzoli, G., Peng, W., Carter, A., Ji, S., and Pan, B.: Loess Plateau storage of Northeastern Tibetan Plateau-derived Yellow River sediment, Nat. Commun., 6, 8511, https://doi.org/10.1038/ncomms9511, 2015.

Ning, Y., Liu, W., and An, Z.: Variation of soil $\delta^{13}C$ values in Xifeng loess-paleosol sequence and its paleoenvironmental implication, Chinese Sci. Bull., 51, 1350–1354, https://doi.org/10.1007/s11434-006-1350-7, 2006.

Pan, B., Pang, H., Gao, H., Garzanti, E., Zou, Y., Liu, X., Li, F., and Jia, Y.: Heavy-mineral analysis and provenance of Yellow River sediments around the China Loess Plateau, J. Asian Earth Sci., 127, 1–11, https://doi.org/10.1016/j.jseaes.2016.06.006, 2016.

Qu, Y., Jin, Z., Wang, J., Wang, Y., Xiao, J., Gou, L.-F., Zhang, F., Liu, C.-Y., Gao, Y., Suarez, M. B., and Xu, X.: The sources and seasonal fluxes of particulate organic carbon in the Yellow River, Earth Surf. Proc. Land., 45, 2004–2019, https://doi.org/10.1002/esp.4861, 2020.

Ran, L., Lu, X. X., Sun, H., Han, J., Li, R., and Zhang, J.: Spatial and seasonal variability of organic carbon transport in the Yellow River, China, J. Hydrol., 498, 76–88, https://doi.org/10.1016/j.jhydrol.2013.06.018, 2013.

Rao, Z., Guo, W., Cao, J., Shi, F., Jiang, H., and Li, C.: Relationship between the stable carbon isotopic composition of modern plants and surface soils and climate: A global review, Earth-Sci. Rev., 165, 110–119, https://doi.org/10.1016/j.earscirev.2016.12.007, 2017.

Repasch, M., Scheingross, J. S., Hovius, N., Lupker, M., Wittmann, H., Haghipour, N., Gröcke, D. R., Orfeo, O., Eglinton, T. I., and Sachse, D.: Fluvial organic carbon cycling regulated by sediment transit time and mineral protection, Nat. Geosci., 14, 842–848, https://doi.org/10.1038/s41561-021-00845-7, 2021.

Rouse, H.: Modern Conceptions of the Mechanics of Fluid Turbulence, T. Am. Soc. Civ. Eng., 102, 463–505, https://doi.org/10.1061/TACEAT.0004872, 1937.

Schwab, M. S., Hilton, R. G., Haghipour, N., Baronas, J. J., and Eglinton, T. I.: Vegetal Undercurrents—Obscured Riverine Dynamics of Plant Debris, J. Geophys. Res.-Biogeo., 127, e2021JG006726, https://doi.org/10.1029/2021JG006726, 2022.

Shi, H. and Shao, M.: Soil and water loss from the Loess Plateau in China, J. Arid Environ., 45, 9–20, https://doi.org/10.1006/jare.1999.0618, 2000.

Shi, H., Wang, X., Xu, M., Zhang, H., and Luo, Y.: Characteristics of soil C : N ratio and $\delta^{13}C$ in wheat-maize cropping system of the North China Plain and influences of the Yellow River, Sci. Rep., 7, 16854, https://doi.org/10.1038/s41598-017-17060-3, 2017.

Stevens, T., Carter, A., Watson, T. P., Vermeesch, P., Andò, S., Bird, A. F., Lu, H., Garzanti, E., Cottam, M. A., and Sevastjanova, I.: Genetic linkage between the Yellow River, the Mu Us desert and the Chinese Loess Plateau, Quaternary Sci. Rev., 78, 355–368, https://doi.org/10.1016/j.quascirev.2012.11.032, 2013.

Stock, B. C. and Semmens, B. X.: brianstock-/MixSIAR 3.1.9 (3.1.9), Zenodo [data set], https://doi.org/10.5281/zenodo.1209993, 2016.

Sun, D., Tang, J., He, Y., Liao, W., and Sun, Y.: Sources, distributions, and burial efficiency of terrigenous organic matter in surface sediments from the Yellow River mouth, northeast China, Org. Geochem., 118, 89–102, https://doi.org/10.1016/j.orggeochem.2017.12.009, 2018.

Syvitski, J. P. M., Vörösmarty, C. J., Kettner, A. J., and Green, P.: Impact of Humans on the Flux of Terrestrial Sediment to the Global Coastal Ocean, Science, 308, 376–380, https://doi.org/10.1126/science.1109454, 2005.

Tao, S., Eglinton, T. I., Montluçon, D. B., McIntyre, C., and Zhao, M.: Pre-aged soil organic carbon as a major component of the Yellow River suspended load: Regional significance and global relevance, Earth Planet. Sci. Lett., 414, 77–86, https://doi.org/10.1016/j.epsl.2015.01.004, 2015.

Tao, S., Eglinton, T. I., Montluçon, D. B., McIntyre, C., and Zhao, M.: Diverse origins and pre-depositional histories of organic matter in contemporary Chinese marginal sea sediments, Geochim. Cosmochim. Ac., 191, 70–88, https://doi.org/10.1016/j.gca.2016.07.019, 2016.

Tao, S., Eglinton, T. I., Zhang, L., Yi, Z., Montluçon, D. B., McIntyre, C., Yu, M., and Zhao, M.: Temporal variability in composition and fluxes of Yellow River particulate organic matter, Limnol. Oceanogr., 63, S119–S141, https://doi.org/10.1002/lno.10727, 2018.

Tipper, E. T., Stevenson, E. I., Alcock, V., Knight, A. C. G., Baronas, J. J., Hilton, R. G., Bickle, M. J., Larkin, C.

S., Feng, L., Relph, K. E., and Hughes, G.: Global silicate weathering flux overestimated because of sediment-water cation exchange, P. Natl. Acad. Sci. USA, 118, e2016430118, https://doi.org/10.1073/pnas.2016430118, 2021.

Turowski, J. M., Hilton, R. G., and Sparkes, R.: Decadal carbon discharge by a mountain stream is dominated by coarse organic matter, Geology, 44, 27–30, 2016.

Walling, D. E. and Fang, D.: Recent trends in the suspended sediment loads of the world's rivers, Global Planet. Change, 39, 111–126, https://doi.org/10.1016/S0921-8181(03)00020-1, 2003.

Wang, C., Li, F., Shi, H., Jin, Z., Sun, X., Zhang, F., Wu, F., and Kan, S.: The significant role of inorganic matters in preservation and stability of soil organic carbon in the Baoji and Luochuan loess/paleosol profiles, Central China, CATENA, 109, 186–194, https://doi.org/10.1016/j.catena.2013.04.001, 2013.

Wang, H., Yang, Z., Saito, Y., Liu, J. P., Sun, X., and Wang, Y.: Stepwise decreases of the Huanghe (Yellow River) sediment load (1950–2005): Impacts of climate change and human activities, Global Planet. Change, 57, 331–354, https://doi.org/10.1016/j.gloplacha.2007.01.003, 2007.

Wang, H., Bi, N., Saito, Y., Wang, Y., Sun, X., Zhang, J., and Yang, Z.: Recent changes in sediment delivery by the Huanghe (Yellow River) to the sea: Causes and environmental implications in its estuary, J. Hydrol., 391, 302–313, https://doi.org/10.1016/j.jhydrol.2010.07.030, 2010.

Wang, H., Wu, X., Bi, N., Li, S., Yuan, P., Wang, A., Syvitski, J. P. M., Saito, Y., Yang, Z., Liu, S., and Nittrouer, J.: Impacts of the dam-orientated water-sediment regulation scheme on the lower reaches and delta of the Yellow River (Huanghe): A review, Global Planet. Change, 157, 93–113, https://doi.org/10.1016/j.gloplacha.2017.08.005, 2017.

Wang, S., Fu, B., Piao, S., Lü, Y., Ciais, P., Feng, X., and Wang, Y.: Reduced sediment transport in the Yellow River due to anthropogenic changes, Nat. Geosci., 9, 38–41, https://doi.org/10.1038/ngeo2602, 2016.

Wang, X., Ma, H., Li, R., Song, Z., and Wu, J.: Seasonal fluxes and source variation of organic carbon transported by two major Chinese Rivers: The Yellow River and Changjiang (Yangtze) River, Global Biogeochem. Cy., 26, GB2025, https://doi.org/10.1029/2011gb004130, 2012.

Wang, X., Xu, C., Druffel, E. M., Xue, Y., and Qi, Y.: Two black carbon pools transported by the Changjiang and Huanghe Rivers in China, Global Biogeochem. Cy., 30, 1778–1790, https://doi.org/10.1002/2016GB005509, 2016.

Xue, D., Lu, J., Leung, L. R., Teng, H., Song, F., Zhou, T., and Zhang, Y.: Robust projection of East Asian summer monsoon rainfall based on dynamical modes of variability, Nat. Commun., 14, 3856, https://doi.org/10.1038/s41467-023-39460-y, 2023.

YRCC: Annual Sediment Report for the Yellow River, Yellow River Conservation Committee, http://www.yrcc.gov.cn/nishagonggao/2016/ (last access: 15 November 2021), 2016.

Yu, M., Eglinton, T. I., Haghipour, N., Montlucon, D. B., Wacker, L., Hou, P., Zhang, H., and Zhao, M.: Impacts of Natural and Human-Induced Hydrological Variability on Particulate Organic Carbon Dynamics in the Yellow River, Environ. Sci. Technol., 53, 1119–1129, https://doi.org/10.1021/acs.est.8b04705, 2019a.

Yu, M., Eglinton, T. I., Haghipour, N., Montluçon, D. B., Wacker, L., Wang, Z., Jin, G., and Zhao, M.: Molecular isotopic insights into hydrodynamic controls on fluvial suspended particulate organic matter transport, Geochim. Cosmochim. Ac., 262, 78–91, https://doi.org/10.1016/j.gca.2019.07.040, 2019b.

Zhang, L. J., Wang, L., Cai, W.-J., Liu, D. M., and Yu, Z. G.: Impact of human activities on organic carbon transport in the Yellow River, Biogeosciences, 10, 2513–2524, https://doi.org/10.5194/bg-10-2513-2013, 2013.

Zhou, W., Xian, F., Beck, J. W., Jull, A. J. T., An, Z., Wu, Z., Liu, M., Chen, M., Priller, A., Kutschera, W., Burr, G. S., Yu, H., Song, S., Cheng, P., and Kong, X.: Reconstruction of 130-kyr Relative Geomagnetic Intensities from $^{10}$Be in Two Chinese Loess Sections, Radiocarbon, 52, 129–147, https://doi.org/10.1017/S0033822200045082, 2010.

Zhu, T. X.: Gully and tunnel erosion in the hilly Loess Plateau region, China, Geomorphology, 153–154, 144–155, https://doi.org/10.1016/j.geomorph.2012.02.019, 2012.